Hugin-AstA circuitry is a novel central energy sensor that directly regulates sweet sensation in *Drosophila* and mouse

Wusa Qin[1,6], Tingting Song[2, 3, 6], Zeliang Lai[4], Daihan Li[3], Liming Wang[1, 2, 3,*], and Rui Huang[3,5,*]

[1]Institute of Molecular Physiology, Shenzhen Bay Laboratory, Shenzhen, 518055, China.

[2]School of Public Health, Capital Medical University, Beijing, 100069, China.

[3]Chinese Institutes for Medical Research, Beijing, 100069, China.

[4] Center for Neurointelligence, School of Medicine, Chongqing University, Chongqing, 400030, China.

[5]Guangyang Bay Laboratory, Chongqing Institute for Brain and Intelligence, Chongqing, 400060, China.

[6]These authors contribute equally to this work.

[*]For correspondence: lmwang83@ccmu.edu.cn; huangrui0716@sina.com

Abstract

Taste sensation plays a crucial role in shaping feeding behavior and is intricately influenced by internal states like hunger or satiety. Despite the identification of numerous neural substrates regulating feeding behavior, the central neural substrate that linked energy-sensing and taste sensation remained elusive. Here, we identified a novel neural circuitry that could directly sense internal energy state and modulate sweet sensation in the Drosophila brain. Specifically, a subset of neuropeptidergic neurons expressing hugin directly detected elevated levels of circulating glucose via glucose transporter Glut1 and ATP-sensitive potassium channel. Upon activation, these neurons released hugin peptide and activated downstream Allatostatin A (AstA)$^{+}$ neurons via its cognate receptor PK2-R1. Subsequently, the activation of AstA^{+} neurons then directly inhibited sweet sensation via AstA peptide and its cognate receptor AstA-R1 expressed in sweet-sensing Gr5a^{+} neurons. We also showed that neuromedin U (NMU), the mammalian homolog of fly hugin, served as an energy sensor to suppress sweet sensation. Therefore, these data identify hugin^{+} neuron as a central energy sensor responsible for regulating sweet sensation across species.

Keywords: satiety, sweet sensation, feeding, hugin, AstA

Introduction

Animal behaviors are tightly associated with the internal metabolic states (Munch et al., 2020). When experiencing hunger, animals exhibit behaviors aimed at obtaining food, including elevated sensitivity to appetitive cues and enhanced foraging and feeding behaviors (Augustine et al., 2020; Marella et al., 2012; Yu et al., 2016). In addition, hunger tends to increase anxiety levels and aggressive behaviors (de Rivaz et al., 2022), while inhibiting pain, sleep, and mating behaviors (Alhadeff et al., 2018; Burnett et al., 2016; Sun et al., 2023). These behavioral alterations upon hunger serve to sharpen the focus of starved animals on the tasks related to food acquisition (Deem et al., 2022). Conversely, when animals are sated, food-related behaviors diminish, redirecting their attention to other important behaviors such as reproduction (Burnett et al., 2016; Karigo and Deutsch, 2022). Such adjustments in behaviors help animals to fulfill various internal needs in a fast-changing environment, and also suggests the presence of neural circuitry in the brain that detects and encodes hunger and satiety states to guide individual behavioral choices and maintain metabolic homeostasis.

In mammals, agouti-related peptide (AgRP)- and pro-opiomelanocortin (POMC)-expressing neurons in the hypothalamic arcuate nucleus (ARC) are key sensors of hunger and satiety (Fu et al., 2019). When calories are scarce, AgRP neurons become active, promoting foraging and feeding behaviors while suppressing competing behaviors such as thirst, innate fear, anxiety-related behavior, and social interactions (Burnett et al., 2016; Dietrich et al., 2015). Conversely, satiety signals gradually inhibit the activity of AgRP neurons in response to food or food cues, resulting in reduced appetite (Bruning and Fenselau, 2023; Chen et al., 2015).

Antagonistic to AgRP neurons, POMC neurons play a critical role as satiety sensors, suppressing feeding and increasing energy expenditure by releasing a α-melanocyte-stimulating hormone (α-MSH) (Bruning and Fenselau, 2023; Koch et al., 2015). AgRP/POMC neuron activity is regulated by various upstream signals, including hormones like leptin, insulin, and ghrelin, as well as nutrients such as glucose, amino acids, and fatty acids. Leptin, GLP-1, and insulin activate POMC neurons while inhibiting AgRP neurons, reducing food intake (Belgardt et al., 2009; De Solis et al., 2024), whereas ghrelin, secreted during fasting, activates AgRP neurons to promote feeding (Vivot et al., 2023). Furthermore, AgRP and POMC neurons project to various brain regions inlcuding paraventricular hypothalamus (PVH), dorsomedial hypothalamus (DMH), ventromedial hypothalamus (VMH), and brainstem, exerting complex regulations on behavior and metabolism (Belgardt et al., 2009; De Solis et al., 2024; Wei et al., 2018). These intertwined circuitry helps to coordinate behaviors and physiological responses in a dynamic environment. Despite the significant progress in the past decades, the direct link of these upstream internal energy sensors, such as AgRP and POMC neurons, to various behavioral outputs, remains incompletely understood. Current research highlights their central role in energy homeostasis but also suggests a complex, multi-level circuitry that modulates these behaviors. Fully elucidating the relative contributions of these neurons and circuits to behavioral and metabolic regulations is an ongoing challenge in the field.

Fruit flies offer an excellent system for studying satiety/hunger sensing and mapping out the complete circuitry towards behavioral consequences, owing to their simple nervous system

82 and comprehensive genetic and neurobiological tools (Lin et al., 2019). Hunger and satiety
83 states modulate a range of behaviors in *Drosophila*, including foraging, feeding, food
84 preference, sleep, and even memory formation (Chouhan et al., 2021; Lin et al., 2019).
85 Hungry flies tend to increase foraging, favor high-calorie food, and extend feeding durations,
86 while satiated flies reduce food intake and shift their food preferences (Lin et al., 2019).
87 Hunger also disrupts sleep, with starved flies becoming more alert to prioritize food-seeking
88 (Willyard, 2008). A constellation of neuromodulators has been shown to steer these
89 behavioral transitions. Dopamine navigates the feeding process by engaging reward pathways
90 upon food detection (Marella et al., 2012), whereas serotonin (5-HT) functions to quell
91 feeding behavior during satiety (Yao and Scott, 2022), simultaneously shaping food
92 preferences and foraging endeavors. Neuropeptide F (NPF), akin to mammalian neuropeptide
93 Y (NPY), is instrumental in instigating feeding bouts during periods of hunger (Malita et al.,
94 2022). Hugin, bearing a resemblance to mammalian neuropeptide U, influences satiety levels
95 and modulates food intake, regulated by gustatory neurons (Melcher and Pankratz, 2005;
96 Schoofs et al., 2014). Short neuropeptide F (sNPF) contributes to hunger-induced behaviors
97 by calibrating sensory reactions to food stimuli (Root et al., 2011). Allatostatin A (AstA)
98 emerges as a satiety signal that, likely through interactions with sweet-sensing neurons, and
99 suppresses feeding activities. (Chen et al., 2016; Hentze et al., 2015; Hergarden et al., 2012).
100 CCHamide, which is associated with growth modulation, potentially acts as a hunger signal,
101 whereas leucokinin adjusts meal size and manages the physiological aftermath of feeding (Lin
102 et al., 2019). Corazonin is perceived to be intertwined with the modulation of stress and
103 metabolic responses pertinent to hunger and satiety (Kubrak et al., 2016). SIFamide is

recognized for its role in translating hunger signals into both appetitive and consummatory feeding actions (Martelli et al., 2017). The intricate interplay among these modulators constitutes a sophisticated regulatory network, the intricacies of which are yet to be delineated comprehensively, underscoring an exciting frontier for forthcoming research aimed at unraveling the neural circuitry that underpins energy homeostasis.

Sugar serves as an important source of satiety signals. The body's precise responses to dietary sugar involve both peripheral organs and the brain, which facilitates the regulation of various behaviors, including sweet perception and food consumption (Oh et al., 2021; Qi et al., 2021; Ugrankar et al., 2018; Zhao et al., 2022). When exposed to a high-sugar diet, the midgut reacts by secreting Hedgehog (Hh) to suppress sweet sensation (Zhao et al., 2022). Additionally, hugin^{+} neurons in the ventral nerve cord (VNC) become sugar-sensitive in fed states, leading to the suppression of food consumption via neuropeptide diuretic hormone 44 (DH44)$^{+}$ neurons(Oh et al., 2021). In the brain, insulin-producing cells (IPCs) and tackykinin (TK)$^{+}$ neurons are also activated in the presence of sugar, contributing to appetite suppression (Hergarden et al., 2012; Lin et al., 2019; Qi et al., 2021). In contrast to satiety sensing, certain neurons, such as dopaminergic neurons, act as hunger sensors in fruit fly brains, being activated during hunger states and involved in regulation of sleep, sugar memory expression and sweet taste sensation (Marella et al., 2012; Senapati et al., 2019; Yurgel et al., 2019). However, it remains unclear how these neurons interact to form a regulatory network on energy homeostasis, especially how these neurons link the hunger/satiety state to direct behavioral outputs.

We aimed to dissect out a complete neural pathway that directly sensed internal energy state and modualted food-related behavioral output in the fly brain. More specifically, we focused on the circuitry mediating the effect of satiety to inhibit sweet taste sensation. Among several candidate neuropeptidergic neuron groups, we pinpointed hugin^{+} neurons as a direct satiety sensor in the fly brain. These hugin^{+} neurons were activated by elevated levels of circulating glucose after feeding, which in turn activated downstream AstA^{+} neurons via the interaction of hugin peptide and its cognate receptor PK2-R1. Subsequently, AstA^{+} neurons exerted direct inhibitory effect on sweet-sensing Gr5a^{+} neurons via AstA peptide and its receptor AstA-R1. As a result, sated flies exhibited a reduction in sweet sensitivity and hence food consumption. In summary, we unveiled a novel satiety sensing mechanism in *Drosophila* that detected circulating glucose and regulated sweet perception and feeding. We also showed that NMU, the mammalian homolog of hugin, was also an energy sensor in mouse models involved in regulation of sweet perception, highlighting the conserved regulatory mechanism of central energy sensing and sweet sensation across species.

142 ## Results

143 ### hugin^{+} neurons were a novel glucose sensor in the fly brain

144 Flies extend their proboscis in response to appetitive cues, a behavioral element known as the
145 proboscis extension reflex (PER) (Marella et al., 2012; Song et al., 2023). As previously
146 observed, hunger significantly enhances this reflex(Marella et al., 2012). In our study, we first
147 replicated this phenomenon: In the state of hunger, flies exhibited elevated PER towards
148 various concentrations of sugar compared to those under fed conditions (***Figure 1A-B***). These
149 results confirmed the notion that sweet sensation was influenced by the internal energy state,
150 elevated by starvation and suppressed by satiety (Inagaki et al., 2014; Marella et al., 2012).
151 Sweet sensation in flies is mediated by sweet-sensing Gr5a^{+} neurons located on the proboscis
152 (Fujii et al., 2015). Consistent with the behavioral effect, we also confirmed that Gr5a^{+}
153 neurons exhibited elevated calcium responses to sugar under starvation conditions (***Figure***
154 ***supplementary 1A***).

155

156 Dopaminergic neurons in the subesophageal zone (SEZ) region of the fly brain acted as a
157 hunger sensor, promoting sweet sensation via a specific dopamine receptor DopEcR
158 expressed in Gr5a^{+} neurons (Inagaki et al., 2014; Marella et al., 2012). However, although the
159 gene knockout of tyrosine hydroxylase (TH) (Budnik and White, 1987), a key enzyme for
160 dopamine biosynthesis, significantly suppressed sweet sensation in starved fruit flies (***Figure***
161 ***supplementary 1B***), these flies still showed a further reduction in sugar-induced PER under
162 sated conditions (***Figure supplementary 1C-D***). These results suggest the existence of
163 dopamine-independent mechanisms for sensing satiety and hunger in fruit flies that exerts

modulatory effect on sweet sensation.

In the terminating phase of feeding behavior, satiety signals play a crucial role to cease food consumption and to ensure an appropriate amount of food ingestion. A number of neuropeptidergic neurons were identified as putative satiety signals (Lin et al., 2019). Notably, some of these neurons, including those secreting neuropeptides LK, TK, hugin, AstA, CCHa1, and CCHa2, are also distributed in the SEZ region (Deng et al., 2019). It has been reported that the sweet-sensing gustatory neurons primarily receive regulatory inputs from neurons in the SEZ region (Marella et al., 2012; Song et al., 2023). Therefore, we hypothesized that these neuropeptidergic neurons might function as satiety signals, imposing inhibititory effect on sweet sensation after adequate food ingestion.

To test this hypothesis, we selectively expressed the temperature-sensitive ion channel TrpA1 in these neurons and activated them at 30 °C, triggering the release of corresponding neuropeptides. Indeed, activation of LK-, TK-, hugin-, AstA-, CCHa1-, and CCHa2-expressing neurons robustly suppressed sweet taste sensitivity in both fed and starved flies (***Figure 1C–D***; ***also see Figure supplementary 2***). Moreover, LK-, TK-, and hugin-expressing neurons exerted particularly strong inhibition under satiated conditions (***Figure 1C–D; also see Figure supplementary 2***). These results reveal a multilayered, state-dependent neuropeptidergic network that finely tunes gustatory processing and feeding behavior. In contrast, activating dopaminergic neurons enhanced sweet perception in sated flies as expected (***Figure 1C***). In starved flies, activating dopaminergic neurons elicited no

186 change in PER likely due to a ceiling effect (***Figure 1D***).

187

188 In mammals and flies, circulating sugar levels are directly linked to satiety/hunger state (Lin
189 et al., 2019; Qi et al., 2021; Yoon and Diano, 2021). We then asked whether changes in
190 circulating sugar levels exerted an effect on sweet sensation. Activating IPCs in the fly brain
191 released *Drosophila* Insulin-like Peptides (DILPs), the fly analog of mammalian insulin
192 (Brogiolo et al., 2001), into the hemolymph and reduced circulating sugar levels (***Figure***
193 ***supplementary 3A***). As a result, such manipulation enhanced sweet sensitivity of fed flies
194 (***Figure supplementary 3B-C***). Therefore, it was plausible that changes in circulating sugar
195 might be the driver of changes in sweet sensation.

196

197 Indeed, allowing starved flies to re-feed on normal fly diet or sucrose alone for 15 minutes
198 both resulted in a significant decrease in sweet sensation (***Figure 1E***). To validate this effect
199 across sweet modalities, we assessed responses to trehalose and fructose after sucrose
200 refeeding and observed comparable reductions in sweet sensation (***Figure supplementary 4***).
201 Conversely, when starved flies were supplied with fly diet deprived of sucrose (but with
202 normal levels of polysaccharides, proteins, and lipids), there was no immediate change in
203 sweet sensation after re-feeding (***Figure 1E***). These results demonstrate that sugar intake
204 inhibits sweet sensation, probably via increasing circulating sugar levels.

205

206 Collectively, we thus hypothesized that the above neuropeptidergic neurons might directly
207 sense an increase of circulating sugar levels and suppress sweet sensation in response. If so,

208 these neurons should be activated by glucose, the main species of circulating sugars
209 associated with feeding behavior in flies (Ugrankar et al., 2018), at the concentrations
210 resembling sated state (>50 mM in fed flies (***Figure supplementary 5***)). We thus conducted
211 calcium imaging experiments in fly brains in an *ex vivo* preparation (Qi et al., 2021). Among
212 all the six groups of neuropeptidergic neurons we examined in the SEZ, only hugin$^+$ neurons
213 and AstA$^+$ neurons could be activated by 50 mM glucose (***Figure 1F-I, also see Figure***
214 ***supplementary 6***). Remarkably, each of these populations subdivided into anatomically
215 distinct SEZ subclusters (***Figure supplementary 7A; Figure supplementary 9A***), yet glucose-
216 evoked Ca^{2+} responses occurred exclusively within a single subcluster (***Figure 1H,I; Figure***
217 ***supplementary 7B; Figure supplementary 9B***). This selective activation highlighted
218 profound functional heterogeneity in nutrient sensing among these neuron groups. When
219 direct synaptic transmission was blocked with TTX, hugin$^+$ neurons, but not AstA$^+$ neurons,
220 still exhibited calcium responses towards 50 mM of glucose (***Figure 1G, green***), suggesting
221 that hugin$^+$ neurons are a direct glucose sensor. Furthermore, the level of circulating glucose
222 dropped to ~ 20 mM in starved flies (***Figure supplementary 5***). We found that 20 mM of
223 glucose did not activate hugin$^+$ and AstA$^+$neurons (***Figure 1G and I, orange***), suggesting that
224 these neurons can only be activated under sated conditions.
225
226 We also assessed the activity of hugin$^+$ neurons *in vivo* using calcium-modulated
227 photoactivatable ratiometric integrator (CaMPARI), a method employing a photoconvertible
228 fluorescent protein that allows the imaging of integrated calcium activity (Fosque et al.,
229 2015), under both sated and starved conditions. In the CaMPARI assay, when neurons are

230 activated, leading to an increase in free calcium ions, exposure to 405-nm light induces a
231 permanent green-to-red photoconversion (Fosque et al., 2015). We found an increased ratio of
232 red/green fluorescence in hugin$^+$ neurons in the sated state compared to that upon starvation
233 (***Figure 1J***). These findings strongly imply that hugin$^+$ neurons function as a direct satiety
234 sensor, sensing the levels of circulating glucose and modulating sweet sensation in response.
235

236 **Glucose activated hugin$^+$ neurons via an ATP-sensitive potassium channel**

237 We then investigated the cellular mechanism through which glucose could directly activate
238 hugin$^+$ neurons. In both mammals and flies, extracellular glucose is usually transported into
239 the cytosol to activate glucose-sensitive neurons (Dus et al., 2015; Oh et al., 2019; Parton et
240 al., 2007). When fly brains were pre-treated with phlorizin, a blocker of glucose transport
241 (Dus et al., 2015; Oh et al., 2019), hugin$^+$ neurons showed diminished calcium responses to
242 glucose, suggesting activation of hugin$^+$ neurons by glucose requires intracellular glucose
243 (***Figure 2A***).
244

245 The transport of glucose mediated by glucose transporter 1 (Glut1) can activate certain
246 neurons in the fruit fly brain (Dus et al., 2015; Oh et al., 2019). By specifically knocking
247 down Glut1 expression in hugin$^+$ neurons, we observed a significant reduction in calcium
248 responses to glucose (***Figure 2B***). Consistently, these flies showed a slight yet significant
249 increase in their PER responses to glucose (***Figure 2C***). Again, these results further confirm
250 that glucose needs to be transported into hugin$^+$ neurons to modulate neuronal activity and
251 behavioral output.

252

253 In pancreatic β-cells and certain fly neurons (Oh et al., 2019; Parton et al., 2007; Wang et al.,
254 2022), intracellular glucose modulates cell excitability primarily through its effect on
255 intracellular energy metabolism and ATP-sensitive potassium channels (K_{ATP}). We pre-treated
256 fly brains with a K_{ATP} inhibitor (glibenclamide) and observed a significant calcium response
257 in hugin$^+$ neurons (***Figure 2D***). Hexokinase, a key enzyme in glucose metabolism that
258 generates ATP, also plays a crucial role in this process. When hexokinase activity was
259 restricted by alloxan, glucose-induced calcium response in hugin$^+$ neurons was significantly
260 suppressed (***Figure 2E***). Similarly, when hexokinase was specifically knocked down in
261 hugin$^+$ neurons, a comparable reduction in glucose-induced calcium responses was observed
262 (***Figure 2F***). Pyruvate, the end product from glycolysis, can lead to ATP generation via the
263 tricarboxylic acid cycle. We also found that pyruvate stimulation led to a significant calcium
264 response in hugin$^+$ neurons (***Figure 2G***). As a specificity control, nonmetabolizable L-glucose
265 failed to activate hugin$^+$ neurons (***Figure 2H***).

266

267 Collectively, these findings suggest that extracellular glucose directly enters hugin$^+$ neurons
268 through specific glucose transporter and subsequently modulate the activity of K_{ATP} through
269 ATP production, ultimately leading to neuronal depolarization.

270

271 **AstA$^+$ neurons were direct downstream target of hugin$^+$ neurons**

272 Since hugin$^+$ neurons were directly involved in glucose sensing and regulated sweet sensation
273 (***Figure 1G and Figure supplementary 8A-B***), we sought to identify their downstream target.

274 We then asked whether the hugin peptide had a direct effect on sweet sensation. Upon
275 microinjection of synthetic hugin peptide, we observed a notable reduction in sweet sensation
276 under both sated and starved states (***Figure 3A***). In line with this observation, following the
277 injection of hugin peptide, we observed a significant reduction of sugar-induced calcium
278 responses in sweet-sensing Gr5a^{+} neurons (***Figure 3B***). Thus, the inhibitory function of
279 hugin^{+} neurons on sweet sensation was likely mediated by the secretion of hugin peptide.
280
281 There were two hugin receptors, PK2-R1 and PK2-R2, in fruit flies (Park et al., 2002). We
282 knocked down their expression by RNAi in the nervous system and then tested flies' PER to
283 sugar. Knocking down PK2-R1 but not PK2-R2 significantly enhanced sweet perception in
284 both sated and starved states (***Figure 3C-D***), suggesting a crucial role of PK2-R1 in receiving
285 the input of hugin^{+} neurons in satiety sensing. To validate this finding, we further tested PK2-
286 R1 null mutants and observed a similar enhancement in sweet sensitivity (***Figure***
287 ***supplementary 10***). Interestingly, we did not observe any expression of PK2-R1 in the
288 proboscis where gustatory sensory neurons were distributed, indicating that sweet-sensing
289 Gr5a^{+} neurons could not directly receive input from hugin^{+} neurons via PK2-R1 (data not
290 shown).
291
292 AstA^{+} neurons served as a plausible relay between hugin^{+} neurons and sweet-sensing Gr5a^{+}
293 neurons, especially based on a clear co-expression of hugin receptor PK2-R1 and AstA in the
294 SEZ region of the fly brain (***Figure 3E***). Notably, these double-labeled neurons corresponded
295 precisely to the AstA subcluster that exhibited glucose-specific Ca^{2+} responses (***Figure 1H***).

We also used optogenetic tools to further confirm that hugin$^+$ neurons acted upstream of AstA$^+$ neurons. We expressed the light-sensitive neuronal activator CsChrimson in hugin$^+$ neurons and calcium indicator GCaMP6m in AstA$^+$ neurons, respectively (Klapoetke et al., 2014). As shown in Figure 3F, opto-activation of hugin$^+$ neurons led to a robust calcium transient in AstA$^+$ neurons.

We then investigated whether the hugin-AstA circuitry affected sweet sensation. As expected, knocking-down PK2-R1 (but not PK2-R2) in AstA$^+$ neurons led to a significant increase in sugar-induced PER (***Figure 3G-H***). Therefore, AstA$^+$ neurons are the direct downstream target of hugin$^+$ neurons in satiety sensing. hugin$^+$ neurons can directly sense elevated circulating glucose levels, promote the release of neuropeptide hugin, and then activate AstA$^+$ neurons via its cognate receptor PK2-R1.

hugin$^+$ neurons are distributed in both the brain and the ventral nerve cord (VNC). The hugin$^+$ neurons in the VNC sense sugar and inhibit feeding behavior by suppressing the activity of DH44 neurons (Oh et al., 2021). To determine which hugin$^+$ neurons regulate the activity of AstA neurons and sweet sensation, we performed the following experiments: 1, Physically severing the neural connection between the brain and the VNC: After severing the neural connection, activation of hugin$^+$ neurons were still able to downregulate the PER behavior, suggesting that hugin neurons in the SEZ regulated sweet perception (***Figure supplementary 11A-B***). 2, Optogenetic experiments in isolated brains: We dissected the fly brains in Figure 3F, and upon light stimulation, we observed a significant calcium response in AstA neurons

318 (***Figure supplementary 11C***). This indicates that hugin$^+$ neurons located in the SEZ but not
319 VNC regulate the activity of AstA neurons. Therefore, we can infer that hugin neurons in the
320 SEZ are responsible for sugar sensing, energy signal transmission, and the output of PER
321 behavior.
322
323 **AstA$^+$ neurons directly inhibited Gr5a$^+$ neurons.**
324 Activation of AstA$^+$ neurons suppressed sweet sensation, resembling the effect of activating
325 hugin$^+$ neurons (Hergarden et al., 2012)(***Figure supplementary 8C-D***). We also evaluated the
326 behavioral effect of AstA peptide. Similar to hugin, the microinjection of AstA resulted in a
327 reduction in sweet sensitivity in fruit flies (***Figure 4A***) and the activity of Gr5a$^+$ neurons
328 (***Figure 4B***). We then speculated whether AstA$^+$ neurons and AstA peptide might function
329 directly on Gr5a$^+$ neurons. The cell bodies of sweet-sensing Gr5a$^+$ neurons are located in the
330 proboscis, whereas their axons extend to the SEZ region of the fly brain (Dahanukar et al.,
331 2007). We observed distributions of the projections of AstA$^+$ neurons and Gr5a$^+$ neurons both
332 in the SEZ region (***Figure 4C***), suggesting that Gr5a$^+$ neurons might directly receive AstA
333 signal in this region.
334
335 AstA has two cognate receptors in fruit flies, AstA-R1 and AstA-R2 (Larsen et al., 2001). Co-
336 labeling experiments in the proboscis confirmed the expression of AstA-R1 in Gr5a$^+$ neurons
337 (***Figure 4D, arrows***), while AstA-R2 was not expressed in the proboscis (data not shown).
338 Functionally, knockdown of AstA-R1 specifically in Gr5a$^+$ neurons, but not that of AstA-R2,
339 significantly enhanced sweet sensation of flies (***Figure 4E-F***). Similar results were observed

340 in AstA-R1 knockout flies (***Figure supplementary 12***).

341

342 Using optogenetic tools, we also confirmed the function of hugin$^+$ neurons and AstA$^+$ neurons

343 on Gr5a$^+$ neurons. Activating hugin$^+$ neurons and AstA$^+$ neurons both significantly reduced

344 sugar-induced responses of Gr5a$^+$ neurons (***Figure 4G-H***). Collectively, these results suggest

345 that satiety-sensing hugin-AstA circuitry can directly modulate sweet sensation of flies via

346 suppressing the activity of Gr5a$^+$ gustatory neurons.

347

348 **hugin–AstA circuitry suppressed food consumption.**

349 Collectively, the hugin-AstA circuitry senses satiety signals and inhibits sweet sensation.

350 Considering the crucial role of sweet sensation in regulating feeding behavior, we

351 hypothesized that hugin-AstA circuitry was also involved in the regulation of food

352 consumption.

353

354 We expressed a temperature-sensitive blocker of synaptic transmission (Shibire^{ts1}) in hugin$^+$

355 neurons or AstA$^+$ neurons (Kitamoto, 2001) and assayed the feeding behavior of flies under

356 both permissive temperature (***Figure supplementary 13A, blue***) and non-permissive

357 temperature (***Figure supplementary 13A, red***). We found that inhibiting the activity of either

358 hugin$^+$ neurons or AstA$^+$ neurons significantly increased food consumption (***Figure***

359 ***supplementary 13B-C***), demonstrating the inhibitory role of the hugin-AstA circuitry on

360 feeding behavior.

361

362 We also examined the role of hugin and AstA receptors in feeding behavior by testing *PK2-R1*
363 and *AstA-R1* gene knockout flies. The results showed that knockout of both receptors
364 enhanced feeding behavior (***Figure supplementary 13D***), consistent with increased sweet
365 perception upon genetic manipulation of these two receptors (***Figure 3-4***). Moreover, these
366 receptor knockout flies exhibited increased lipid storage, which was likely a consequence of
367 their enhanced feeding behavior (***Figure supplementary 13E***). Additionally, we knocked
368 down the expression of AstA-R1 in sweet sensing $Gr5a^{+}$ neurons, and found that these flies
369 exhibited a significant increase in food consumption (***Figure supplementary 13F***), also likely
370 due to the enhanced sweet sensation (***Figure 4E***).
371

372 **Mammalian homolog of hugin was also a putative satiety sensor**

373 Our present work identified hugin-AstA circuitry as a novel satiety sensor and feeding
374 suppressor in fruit flies. Fruit flies and mammals share highly conserved regulatory elements
375 on feeding behavior and energy homeostasis (Song et al., 2023; Stocker, 2004; Yarmolinsky et
376 al., 2009). We thus asked whether this novel satiety-sensing mechanism was also conserved in
377 the mammalian system,
378

379 In rodent models, neuromedin U (NMU), a analogues of hugin, was also found to be an
380 appetite suppressor (Melcher et al., 2006; Schlegel et al., 2016). We found that synthetic
381 NMU could suppress sweet perception when injected into flies' thorax (***Figure***
382 ***supplementary 14***), highlighting the analogy of fly hugin and mammalian NMU. In mouse
383 models, we observed a significant increase in NMU levels in the blood following glucose

384 feeding (***Figure 5A***). Using the sucrose preference test (SPT) to measure sweet preference,
385 we noted that NMU injection reduced sugar preference in mice, phenocopying the effect of
386 glucose feeding (***Figure 5B-C***). Conversely, NMU knockout enhanced sweet sensation in
387 mice (***Figure 5D***). These data demonstrated that both NMU gene and protein plays a crucial
388 role in regulation of sweet sensation.
389
390 Neuropeptide NMU is secreted by a group of neurons located in the VMH region of
391 hypothalamus (Melcher et al., 2006). To investigate whether NMU^+ neurons functioned as an
392 energy sensor in the mouse brain, we injected AAV-EF1α-DIO-GCaMP6m-WPRE into the
393 VMH of NMU-Cre mice, specifically expressing GCaMP6m in NMU^+ neurons. We then
394 monitored the dynamic activity of VMH^{NMU} neurons during glucose stimulation by using
395 fiber photometry (***Figure 5E***). As expected, these neurons showed significant calcium
396 responses following glucose administration in mice (***Figure 5F-G***). To confirm the specificity
397 of GCaMP6m expression in NMU^+ neurons, we co-expressed a Cre-dependent mCherry
398 reporter in the VMH of NMU-Cre mice and performed fluorescence in situ hybridization for
399 NMU mRNA. Colocalization analysis demonstrated that GCaMP6m fluorescence was
400 restricted exclusively to NMU^+ cells (***Figure supplementary 15A***).
401
402 Next, we conducted calcium imaging of brain slices *in vitro* to further assess these neurons'
403 ability to sense glucose (***Figure 5H***). Similar to hugin neurons in the fly brain, VMH^{NMU}
404 neurons in the mouse brain exhibited strong calcium responses to glucose stimulation, which
405 could not be inhibited by TTX (***Figure 5I***), indicating their direct glucose-sensing capability.

406 Also similar to flies, glucose activated these mouse neurons via entering the cells and
407 modulating K_{ATP} channels, as evidenced by the inhibition of calcium responses by alloxan and
408 phlorizin (***Figure 5J***).
409
410 Calbindin 2-positive neurons (Calb2) in the rostral nucleus of the solitary tract (rNST)
411 selectively respond to sweet tastants, facilitating sweet signal from the periphery into the
412 brain (Jin et al., 2021). Because attenuated sweet sensation should correspondingly diminish
413 central sweet-signal transmission, we asked whether NMU modulates this relay. To assess
414 potential anatomical connectivity between VMH NMU^+ neurons and rNST $Calb2^+$ neurons,
415 we employed a dual-virus tracing strategy. In NMU-Cre mice, we injected AAV9-EF1α-DIO-
416 EGFP into the VMH, which revealed dense GFP^+ projections in close apposition to $Calb2^+$
417 neurons in the rNST (***Figure supplementary 15B***). To further confirm this projection is
418 monosynaptic, we combined anterograde tracing by co-injecting AAV2/1-EF1α-DIO-EGFP
419 into the VMH and AAV2/1-hsyn-SV40-NLS-Cre into the rNST. This approach yielded GFP
420 expression in rNST $Calb2^+$ neurons, supporting a direct VMH→rNST NMU^+→$Calb2^+$
421 synaptic link (***Figure 5K***).
422
423 To evaluate the functional consequence of NMU on $Calb2^+$ neuronal activity during sweet
424 stimulation, we delivered AAVs encoding Cre-dependent GCaMP6m into the rNST of Calb2-
425 Cre mice, thereby enabling real-time calcium imaging in $Calb2^+$ neurons (***Figure***
426 ***supplementary 15C***). Using fiber photometry, we recorded calcium responses to sugar
427 stimuli, both with and without NMU injection (***Figure 5L***). We found that NMU injection

428 significantly suppressed the calcium responses to sugar, aligning with observed behavioral
429 phenotypes (***Figure 5M***). These data indicated that the neuropeptide NMU plays a role in
430 regulating sweet taste perception during sugar feeding.
431
432 These findings indicate that NMU^+ neurons can indeed be a putative satiety sensor in the
433 mouse brain that suppresses sweet perception, shedding light on understanding the conserved
434 neural mechanism of feeding regulation in mammals including human.
435

Discussion

In summary, we identified hugin-AstA circuitry as a novel satiety sensor in the fly brain. It directly detects circulating sugar levels, inhibits sweet taste perception, and terminates feeding, helping to maintain the homeostasis of internal energy state (***Figure supplementary 16***). Previous research has shown that hugin^{+} neurons project to the pharyngeal muscles and the ring gland, playing a role in regulating both feeding and sleep，and these neurons are also part of a neural circuit that modulates taste-mediated feeding behavior. (Melcher and Pankratz, 2005; Miroschnikow et al., 2020; Oh et al., 2021). AstA^{+} neurons convey carbohydrate-satiety signals and shift dietary preference from sugar to protein (Hentze et al., 2015; Hergarden et al., 2012). . However, it was unclear whether they could sense the body's energy state, how they interacted with each other, or how they influenced sensory/motor neurons to regulate feeding. Our research has clarified the relationship between hugin and AstA: hugin functions upstream, sensing glucose, while AstA acts downstream, directly modulating sweet-sensing Gr5a^{+} neurons to regulate sugar perception and feeding behavior. This discovery establishes a mechanistic link between glucose sensing and sweet sensation regulation, enhancing our understanding of how energy states influence nutrient sensing and feeding behavior.

Recent studies have highlighted the complex interplay of neural circuits and neuropeptides that regulate satiety and feeding behavior in Drosophila. For instance, dopaminergic and neuropeptide F (NPF) circuits play crucial roles in modulating the activity of Gr5a^{+} sweet-sensing neurons during hunger and refeeding. These studies showed that dopamine signaling

458 adjusts the temporal integration of PER-driving inputs under fed conditions, while NPF
459 enhances Gr5a sensitivity during starvation (Inagaki et al., 2012; Inagaki et al., 2014; Marella
460 et al., 2012). Our findings complement these established mechanisms by identifying the
461 hugin–AstA pathway as a central satiety sensor that directly detects circulating glucose levels
462 and inhibits sweet taste perception to prevent overconsumption. Moreover, the hugin–AstA
463 circuitry fits within a broader regulatory framework of satiety signaling in Drosophila .
464 Peripheral satiety signals, such as enteroendocrine NPF^+ cells, detect luminal sugar and
465 suppress feeding via hormonal release (Malita et al., 2022). Central hunger circuits, including
466 dopaminergic neurons, adjust Gr5a responsiveness according to the energy state (Inagaki et
467 al., 2012). Our study reveals that the hugin–AstA loop acts as a central brake on Gr5a activity
468 following sugar intake, thus closing a feedback loop that protects against excessive sugar
469 ingestion. Together, these multilayered mechanisms—from gut to brain—ensure robust
470 regulation of sweet perception and energy balance.
471
472 Although multiple regulatory elements of energy homeostasis have been identified in both
473 flies and mammals, our present work reveals a novel mechanism that links energy sensing to
474 taste modulation. The energy sensor comprises three types of neurons: $hugin^+$ neurons as the
475 sensor, $AstA^+$ neurons as a relay, and sweet-sensing $Gr5a^+$ neurons as the behavioral
476 modulator. Given the highly conserved regulatory mechanism of energy homeostasis across
477 animal species (***Figure 5A-D***), our work paves a way to fully understand how internal state
478 sensing and behavioral alternations are tightly coupled in more complex organisms, and how
479 they are disrupted in metabolic disorders.

In addition to the novel mechanism we have uncovered in *Drosophila*, it is interesting to consider how conserved these pathways might be in more complex organisms like mammals, particularly concerning the function of the mammalian homologues, NMU (Melcher et al., 2006). NMU is known to play critical roles in regulating energy homeostasis, feeding behavior, insulin secretion, and immune responses in mammals (Teranishi and Hanada, 2021). Our study has shown that NMU neurons may serve as an energy sensor in mammals as well, which regulated nutrient sensing, much like the hugin neurons in *Drosophila*. Given the functional parallels between the hugin-AstA circuitry in flies and NMU signaling in mammals, it is plausible that NMU may interfere with taste signaling to the brain and modulate the brain's reward circuits, affecting other behaviors beyond feeding.

Additionally, our findings open up the possibility of using NMU or its pathways as therapeutic targets for appetite suppression and obesity treatment. Recent developments in appetite-regulating peptides, such as glucagon-like peptide 1 (GLP-1) receptor agonists, have shown efficacy in reducing food intake and promoting weight loss in humans (Aldawsari et al., 2023). Given NMU's role in suppressing sweet taste perception and energy regulation, the NMU system could be a complementary or alternative target for anti-obesity interventions. Exploring how modulating NMU activity could synergize with GLP-1 therapies may provide new strategies for controlling appetite and managing energy balance.

In conclusion, our discovery of the hugin-AstA circuitry in flies provides a foundation for

502 understanding the broader principles of energy sensing and behavioral regulation across
503 species. Further studies in mammals will be essential to explore the potential roles of NMU
504 neurons in these processes and their therapeutic relevance in metabolic disorders.
505
506
507

Materials and methods

Animals

Fly: Flies were maintained on a standard fly diet under conditions of 60% humidity and 25 °C with a 12-hour light and 12-hour dark cycle. Virgin female flies were chosen immediately after emerging and housed in standard fly food (ND) vials, with 20 flies per vial, for a period of 5-6 days before experiments. For temperature-sensitive manipulations (dTrpA1, Shibire^{ts}), flies were reared at 18 °C for 7–8 days, then transferred to 30 °C for 30 min to activate or inhibit targeted neurons; behavioral assays (PER or feeding) were conducted continuously at 30 °C. For starvation, the flies were kept on 2 % Agar for 12-hour.

The following UAS-RNAi lines: *UAS-AstA-R1 RNAi* (#27280), *UAS-AstA-R2 RNAi* (#25935), *UAS-PK2-R1 RNAi (#29624)*, *UAS-PK2-R2 RNAi (#28781)*, *UAS-CD8-GFP*, *LexAop-CD2-RFP (#67093)*, *UAS-GCaMP6m* (*#42748*), *UAS-CaMPARI* (*#58764*), Gr5a-GAL4 (*#57592*), *Gr5a-LexA* (#93014), *ilp2-GAL4 (#37516)*, *elav-GAL4 (#25750)* were obtained from the Bloomington Drosophila Stock Center at Indiana University. *TH-KO*, and all the other Gal4 and LexA lines were from Yi Rao (Deng et al., 2019) (Capital Medical University, Beijing). *UAS-dTrpA1* and *UAS-Shibire^{ts1}* were from David Anderson (Caltech). *UAS-GCaMP6m; LexAop-CsChrimson* was from Yufeng Pan (Southeast University, Nanjing). *LexAop-Chrimson* was from Wei Zhang (Tsinghua University, Beijing).

Mouse: Male C57BL/6J mice at the age of four weeks were procured from cyagen. The mice were kept in standard laboratory conditions at a temperature of 25 ℃ with a 12:12 light/dark

cycle. All experimental procedures were conducted in compliance with the guidelines set by the Laboratory Animal Welfare and Ethics Committee of Chongqing University (CQU-IACUC-RE-202401-004), adhering to both national and international standards.

Behavioral assays (Fly)

PER was evaluated using a method outlined in a previous study. Briefly, individual flies were gently aspirated and positioned in a 200 μL pipette tip, allowing only the head and proboscis to protrude while the dorsal thorax was lightly affixed to prevent escape. After a 3-minute acclimation period, each fly was first presented with 0.5 μL water droplets on the labellum twice. Flies that responded by extending their proboscis were allowed to drink and were subsequently excluded from the experiment. Flies that did not extend their proboscis in response to water were then stimulated sequentially with ascending sucrose concentrations (6.25–800 mM). Each concentration was delivered as two brief (<1 s) touches of a 0.5 μL droplet to the labellum, immediately withdrawn to prevent ingestion. A full proboscis extension, defined as the complete uncoiling of the rostrum beyond the labellum plane, was scored as positive. Partial or delayed (>1 s) extensions were not considered positive responses. Responsiveness at each concentration was recorded if at least one full extension occurred in the two trials.For Figure supplementary 11, the connection between the brain and VNC were cut off by a dissecting scissors before the PER assay.

Feeding was assessed as previously described (Sun et al., 2017). Briefly, 5-day-old flies underwent a 12-hour starvation period on 2% agar and were then moved to a new vial with

test food containing 0.5% Brilliant Blue (MACKLIN, China) for 10 minutes. After a rapid freeze at -20 °C, flies were decapitated in PBS, homogenized, and centrifuged (13,000 g * 5 min). The resulting supernatants were diluted with PBS to a total volume of 1 ml, and absorbance was measured at 620 nm.

Sucrose Preference Test

The two-bottle preference (TBP) behavioral test was conducted in a standard mouse cage. Two bottles, one containing water and the other with a 10 mM sucrose solution, were placed on top of the cage. Each tested mouse was individually caged and adopted to two bottles containing distilled water or a 10 mM sucrose solution for one week. Throughout the training period, the positions of the bottles were alternated every 24 hours to mitigate potential position-related biases. Prior to the TBP tests for sucrose, mice underwent a 12-hour pre-starvation period, followed by re-fed sucrose (20%) for 1 hour or intraperitoneal (IP) administration of NMU (YFLFRPRN-NH_2, 4.5 μm/kg). The consumption of water and sucrose solution over a 2-hour period was meticulously recorded. The sweetener preference ratio was then calculated by dividing the weight of sweetener consumed by the weight of water consumed.

NMU measurement

Blood was obtained from the lower jaw of the mice and clotted at room temperature for 1 hour. The samples were then centrifuged (1,500g, 4 °C) for 10 minutes and the supernatants were collected for NMU measurement. All the manipulations were according to the

manufacturer's instructions (BMASSY,74030).

Hemolymph extraction and glucose measurement

Groups of 40 ice-anesthetized flies were decapitated and placed into a perforated 0.5 ml tube, which was nested inside a 1.5 ml collection tube. Samples were centrifuged at 2,500 × g for 10 min at 4 °C, yielding approximately 2 µl of hemolymph per batch. Hemolymph was pooled to 4 µl per assay (n = 8 independent samples per group) and immediately analyzed for glucose concentration using the Solarbio BC2500 kit (Solarbio, China) according to the manufacturer's instructions.

Microinjection

Flies were delicately positioned and secured within a 200 ml pipette tip, ensuring their heads were directed toward the tip's end. Subsequently, the tip was opened by cutting, exposing the heads and a section of the thorax. About 20 nl of sterile saline, either with or without synthesized peptides (hugin: SVPFKPRL-NH_2, 1 mg/ml (1.1 mM); AstA: LPVYNFGL-NH_2, 1mg/ml (1.1 mM); NMU: YFLFRPRN-NH_2, 1mg/ml (0.9 mM); Control peptide: DYKDDDDKYPYDVPDYA, 1mg/ml (0.48 mM), were injected into the thorax of these flies using a glass micropipette and a microinjector (3-000-207, Drummond Scientific Company Instruments). The glass micropipette was created from thick-walled borosilicate capillaries (3-000-203-G/X, Drummond Scientific Company Instruments).

Immunofluorescence staining

Fly brains were carefully dissected in PBS on ice and then fixed in 4% formaldehyde for 60 minutes. Following fixation, the brains underwent permeabilization and blocking using Dilution/Blocking Buffer (PBS containing 10% Calf Serum and 0.5% Triton X-100) for 2 hours at room temperature. Subsequently, the samples were immersed in the appropriate primary antibodies in Dilution/Blocking Buffer for 24 hours at 4 °C. Afterward, the samples were subjected to a 60-minute wash with Washing Buffer (0.5% Triton X-100 in PBS) four times at room temperature and were then incubated with secondary antibodies for 24 hours at 4 °C. The samples underwent three additional washes with Washing Buffer before being mounted in Fluoroshield (Sigma-Aldrich).

Images were acquired using a scanning confocal microscope with Olympus objectives (20× /0.7 and 40× /0.95w). Antibodies were employed at the following dilutions: mouse anti-nc82 (1:100, DSHB), rabbit anti-GFP (1:500, Abcam), Alexa Fluor 647 goat anti-mouse (1:500, Invitrogen), and Alexa Fluor 488 goat anti-rabbit (1:500, Invitrogen).

In situ hybridization

Mice were anesthetized and perfused with 4% paraformaldehyde (PFA) dissolved in phosphate-buffered saline (PBS, pH 7.4). Brains were carefully removed from the skull and post-fixed in 4% PFA at 4 °C overnight. Subsequently, the brains were transferred to a 20% sucrose solution (in 1 × PBS) at 4 °C until they were ready for sectioning. Twenty-micrometer-thick sections were obtained using a cryostat. The detection of nmu was performed using a fluorescent in situ hybridization technique (RNAscope, Pinpoease)

according to the manufacturer's instructions. Sections were mounted on SuperFrost Plus Gold slides (ThermoFisher) and briefly rinsed in autoclaved Millipore water. They were then subjected to gradient dehydration in 50%, 75%, and 100% ethanol for 5 minutes each. A hydrophobic barrier was created around the sections using an ImmEdge hydrophobic barrier pen (Cat No. 310018). All incubation steps were carried out at 40 °C using the Pinpoease hybridization system (Cat No. SH-08). The subsequent hybridization, amplification, and detection steps were performed strictly according to the manufacturer's instructions.

Stereotaxic brain surgeries and viral injection

Mice were anesthetized with 1-2% isoflurane during stereotaxic injections, performed using a small animal stereotaxic instrument (RWD Life Science, #68030). Throughout the surgery, core body temperature was maintained at 36 ± 1 °C using a feedback-controlled heating system. Micro scissors were used for the incision, and a dental drill was employed to create the cranial window. Viral injections were delivered using a glass microelectrode syringe pump (RWD Life Science, #R-480). To express GCaMP6m and mCherry AAV2/9-EF1α-DIO-GCaMP6m-WPRE (titer: 2.89×10^{12}, #H4955, Obio Biotechnology, Shanghai, China, Co., Ltd.) and AAV2/9-EF1α-DIO-mCherry-WPRE (titer: 2.89×10^{12}, Obio Biotechnology, Shanghai, China, Co., Ltd.) were bilaterally injected into the VMH and rNST, with approximately 0.15 μL of virus delivered per site. The microelectrode was left in place for 10 minutes post-injection before being withdrawn. Injection coordinates were as follows: VMH (AP, −1.46 mm; ML, ±0.4 mm; DV, −5.5 mm) and rNST (AP, −7.08 mm; ML, ±0.6 mm; DV, −4.3 mm). After 3 weeks of AAV injections, optical fibers were chronically implanted in the

VMH or rNST and secured with dental cement (C&B Metabond®, Parkell, Japan). Injection coordinates were determined based on the 4th edition of the mouse brain atlas by Franklin and Paxinos (2008). Mice were allowed to recover for 5-7 days post fiber-implanted before any behavioral or calcium imaging evaluations were conducted. After the experiments, mice were perfused to verify virus expression and fiber placement. Data from mice with poor viral expression or incorrect fiber placement (0-20% of cases) were excluded from the final analysis.

For the anterograde tracing experiments, two viral vectors were used. AAV2/1-hsyn-DIO-EGFP-WPRE (titer: 1×10^{13} viral particles/mL,Obio Biotechnology) was injected into the ventromedial hypothalamus (VMH), and AAV2/1-hsyn-SV40 NLS-Cre (titer: 2.1×10^{12} viral particles/mL, Brain Case) was injected into the rostral nucleus of the solitary tract (rNST). Approximately 0.15 μL of virus was delivered per injection site. After 3 weeks, the brains were perfused and fixed. Subsequently, the brain tissues were sliced and subjected to antibody staining. The fluorescence signals were then recorded and analyzed.

Optical-fiber-based calcium recording in freely mice

Following injection of an AAV2/9-EF1α-DIO-GCaMP6m-WPRE viral vector, an optical fiber (200 μm O.D., 0.37 numerical aperture, Inper Inc., China) was placed 150 μm above the viral injection site. GCaMP6m^{+} mice were implanted with the optic fiber 3 weeks post-AAV injection and allowed to recover for 5–7 days prior to experimental testing.

For Figure 5K-L, mice were first trained to lick glucose (500 mM) from a petri dish. After

training, they were fasted for 12 hours and then received an injection of synthetic NMU peptide, followed by a 30-minute waiting period. During the experimental session, the mice were given 10 seconds to lick glucose from the petri dish while undergoing fiber photometry recording. For Figure 5E-G, mice were fasted for 4 hours and then administered glucose via gastric infusion, with fiber photometry recordings capturing the process. Fluorescence signals were acquired using a dual-channel fiber photometry system (410 nm & 470 nm, RWD Life Science). The laser power at the tip of the optical fiber was kept below 20 μW for both the 470 nm and 410 nm channels to minimize bleaching. ΔF / F was calculated as (470 nm signal - fitted 410 nm signal) / fitted 410 nm signal. Data analysis was performed using software from RWD Life Science.

Ex vivo calcium imaging

For Figure 1G, 1I, figure supplementary 6, and Figure 2freshly dissected fly brains were placed in the sugar-free AHL buffer (108 mM NaCl, 8.2 mM $MgCl_2$, 4 mM $NaHCO_3$, 1 mM NaH_2PO_4, 5 mM KCl, 2 mM $CaCl_2$, 5 mM HEPES, pH 7.3). Baseline recordings of the samples in AHL buffer were taken over 1 minutes. Subsequently, the solutions were added with 100 μM glibenclamide (***Figure 2D***), 50 mM pyruvate (***Figure 2G***) or switched to AHL + glucose (50 mM) with or without indicated chemicals (***Figure 2 A and E***, 1 mM phlorizin or 10 um alloxan), and the pH was adjusted back to 7.3 through gentle perfusion for 3 minutes. Solution flow in the perfusion chamber was controlled by a valve commander (Scientific Instruments). Following stimulation, samples were washed out again with AHL. For the TTX test, 2 μM TTX was added to the AHL solution. Prior to the assay, the samples were pre-

treated with 2 mM TTX for 15 minutes.

For Figure 5H-J, mice (6-9 weeks of age) were deeply anesthetized by avertin (1.25% avertin, 0.2 ml/10g) . Mouse brains were quickly extracted following decapitation and immediately placed in ice-cold slicing buffer (110 mM Choline Cl, 2.5 mM KCl, 1 mM NaH_2PO_4, 25 mM $NaHCO_3$, 5 mM glucose, 7 mM $MgCl_2$, 0.5 mM $CaCl_2$,1.3mM Na ascorbate,0.6mM Na pyruvate bubbled with 95% oxygen and 5% CO_2 with an adjusted pH of 7.3). The brains were then sectioned into 200 μm slices using a vibratome (Leica VT1200S). These slices were incubated artificial cerebrospinal fluid (aCSF) (125 mM NaCl, 2.5 mM KCl, 1 mM NaH_2PO_4, 25 mM $NaHCO_3$, 5 mM glucose, 1.3 mM $MgCl_2$, 2 mM $CaCl_2$,1.3mM Na ascorbate, 0.6 mM Na pyruvate bubbled with 95% oxygen and 5% CO_2 with an adjusted pH of 7.3) at 34 °C for 20 minutes, then transferred to a room temperature for 30 minutes before recording. For Ca^{2+} imaging, the slices were placed in a recording chamber in the low sugar aCSF (125 mM NaCl, 2.5 mM KCl, 1 mM NaH_2PO_4, 25 mM $NaHCO_3$, 1 mM glucose, 1.3 mM $MgCl_2$, 2 mM $CaCl_2$, 1.3 mM Na ascorbate, 0.6mM Na pyruvate, pH 7.3) for 10 minutes (maintained the flow rate for 1-3 ml/ minute). Baseline recordings, perfusion, and Ca^{2+} recording were performed as detailed above.

All imaging was conducted on an Olympus confocal microscope (FVMPE-RS) with a water immersion objective lens (25× /1.05w MP). Image analyses were performed using ImageJ to calculate the mean intensity of the indicated neuron targeting ROIs, and then plotted in Excel (Microsoft). Ratio changes were calculated using the formula: $\Delta F / F = [F - F_0] / F_0$, where F represents the mean fluorescence of the cell body, and F_0 is the average baseline (before

stimulation).

Optogenetics and in vivo calcium imaging

Newly emerged virgin female flies were housed in a fresh vial with standard medium for 3 days and subsequently moved to a vial containing regular food supplemented with 400 μM all-trans-retinal (Sigma R2500) for 2-4 days prior to experiments. These flies were then immobilized on ice, affixed to transparent tape, and the dorsal cuticle of the fly head was delicately removed with forceps to expose the brain, which was immersed in AHL.

For Figure 3F, an array of red LED (Thorlabs, M625L3) was positioned above the brain. Calcium signals of $Gr5a^{+}$ neurons were captured for 60 frames (1 second per frame) in the absence of light to establish a baseline. Subsequently, the next 20 frames were recorded during opto-activation with the light (the light was switched on for 0.45 second and rested for 0.55 second per activation cycle, and the images were collected in rest time), followed by another 60 frames recorded without light afterward.

For Figure 4G and 4H, to apply liquid food (5% sucrose) to the proboscis, a pipette was filled with the taste solution and placed a few microns from the proboscis tip by using a micromanipulator (MP225, Sutter Instruments) prior to recording. Then, we recorded calcium signals for 60 seconds in the absence of light to establish a baseline (1 second per frame). To activate neurons expressing CsChrimson, a red LED was positioned above the brain, controlled by a custom computer program during opto-activation (0.45 second on and 0.55

second off from 60 second to 120 second). The pipette was placed on the proboscis from 80 second to 85 second. Calcium signals of Gr5a^{+} neurons were recorded throughout these processes (1 second per frame).

Image analyses about relative fluorescence changes ΔF / F were performed as ex vivo calcium imaging.

Optogenetics and ex vivo calcium imaging

For Figure supplementary 11C, newly emerged virgin female flies were housed in a fresh vial with standard medium for 3 days and subsequently moved to a vial containing regular food supplemented with 400 µM all-trans-retinal (Sigma R2500) for 2-4 days prior to experiments. The brains were dissected and placed under a red LED. Calcium signals of AstA^{+} neurons were recorded with or without LED light as above. Image analyses were performed as ex vivo calcium imaging.

Calcium imaging with CaMPARI

The flies were then gently immobilized on ice, attached to transparent tape, and the dorsal cuticle of the fly head was carefully removed with forceps to expose the brain, which was immersed in AHL. Photoconversion (PC) was achieved for 30 seconds using a 405 nm LED [Thorlabs, M405L2–UV (405 nm) Mounted LED, 1,000 mA, 410 mW], controlled by a LED controller (Thorlabs, LEDDB1 driven with 1000 mA). Images were captured using an Olympus confocal microscope. Image analyses were performed in ImageJ by manually

drawing ROIs covering individual neuronal cell bodies using the green channel. The extent of CaMPARI photoconversion was determined as the Red: Green ratio.A '-405 nm' control was included to demonstrate that scanning of the hugin neurons without exposure to ultraviolet light does not convert green to red fluorescence.

Statistical analysis

Data are shown as means (± SEM). Data presented in this study were verified for normal distribution by D'Agostino–Pearson omnibus test. Student's t test, one-way ANOVA and two-way ANOVA (for comparisons among three or more groups and comparisons with more than one variant) were used. The post hoc test with Bonferroni correction was performed for multiple comparisons following ANOVA.

Acknowledgements

We express gratitude to all members of the Wang and Huang Lab for their valuable discussions and technical support. Special thanks to Yi Rao and Bowen Deng for generously providing *Drosophila* chemoconnectome lines, and to Yulong Li and Jianzhi Zeng for their assistance with *in vivo* calcium imaging preparations. Appreciation is extended to the members of the Neuroscience Pioneer Club for their insightful discussions throughout the course of this study. This study was funded by the National Natural Science Foundation of China (No. 32071006 for L.W. and No. 32271008 for R.H.), Guangdong Basic and Applied Basic Research Foundation (2023A1515110454 for T.S.), and the startup funds from Shenzhen Bay Laboratory and Chinese Institutes for Medical Research to L.W.

Author contributions

T.S., R.H., and L.W. designed the experiments and wrote the manuscript. W.Q., and T.S. conducted and analyzed all the experiments. L.W. and R.H. supervised the project.

Competing interests

The authors declare no competing interest.

References

Aldawsari, M., Almadani, F.A., Almuhammadi, N., Algabsani, S., Alamro, Y., and Aldhwayan, M. (2023). The Efficacy of GLP-1 Analogues on Appetite Parameters, Gastric Emptying, Food Preference and Taste Among Adults with Obesity: Systematic Review of Randomized Controlled Trials. Diabetes Metab Syndr Obes *16*, 575-595.

Alhadeff, A.L., Su, Z., Hernandez, E., Klima, M.L., Phillips, S.Z., Holland, R.A., Guo, C., Hantman, A.W., De Jonghe, B.C., and Betley, J.N. (2018). A Neural Circuit for the Suppression of Pain by a Competing Need State. Cell *173*, 140-152 e115.

Augustine, V., Lee, S., and Oka, Y. (2020). Neural Control and Modulation of Thirst, Sodium Appetite, and Hunger. Cell *180*, 25-32.

Belgardt, B.F., Okamura, T., and Bruning, J.C. (2009). Hormone and glucose signalling in POMC and AgRP neurons. J Physiol *587*, 5305-5314.

Brogiolo, W., Stocker, H., Ikeya, T., Rintelen, F., Fernandez, R., and Hafen, E. (2001). An evolutionarily conserved function of the Drosophila insulin receptor and insulin-like peptides in growth control. Curr Biol *11*, 213-221.

Bruning, J.C., and Fenselau, H. (2023). Integrative neurocircuits that control metabolism and food intake. Science *381*, eabl7398.

Budnik, V., and White, K. (1987). Genetic dissection of dopamine and serotonin synthesis in the nervous system of Drosophila melanogaster. J Neurogenet *4*, 309-314.

Burnett, C.J., Li, C., Webber, E., Tsaousidou, E., Xue, S.Y., Bruning, J.C., and Krashes, M.J. (2016). Hunger-Driven Motivational State Competition. Neuron *92*, 187-201.

Chen, J., Reiher, W., Hermann-Luibl, C., Sellami, A., Cognigni, P., Kondo, S., Helfrich-Forster,

802 C., Veenstra, J.A., and Wegener, C. (2016). Allatostatin A Signalling in Drosophila Regulates
803 Feeding and Sleep and Is Modulated by PDF. PLoS Genet *12*, e1006346.
804 Chen, Y., Lin, Y.C., Kuo, T.W., and Knight, Z.A. (2015). Sensory detection of food rapidly
805 modulates arcuate feeding circuits. Cell *160*, 829-841.
806 Chouhan, N.S., Griffith, L.C., Haynes, P., and Sehgal, A. (2021). Availability of food
807 determines the need for sleep in memory consolidation. Nature *589*, 582-585.
808 Dahanukar, A., Lei, Y.T., Kwon, J.Y., and Carlson, J.R. (2007). Two Gr genes underlie sugar
809 reception in Drosophila. Neuron *56*, 503-516.
810 de Rivaz, R., Swendsen, J., Berthoz, S., Husky, M., Merikangas, K., and Marques-Vidal, P.
811 (2022). Associations between Hunger and Psychological Outcomes: A Large-Scale
812 Ecological Momentary Assessment Study. Nutrients *14*.
813 De Solis, A.J., Del Rio-Martin, A., Radermacher, J., Chen, W., Steuernagel, L., Bauder, C.A.,
814 Eggersmann, F.R., Morgan, D.A., Cremer, A.L., Sue, M.*, et al.* (2024). Reciprocal activity of
815 AgRP and POMC neurons governs coordinated control of feeding and metabolism. Nat Metab
816 *6*, 473-493.
817 Deem, J.D., Faber, C.L., and Morton, G.J. (2022). AgRP neurons: Regulators of feeding,
818 energy expenditure, and behavior. FEBS J *289*, 2362-2381.
819 Deng, B., Li, Q., Liu, X., Cao, Y., Li, B., Qian, Y., Xu, R., Mao, R., Zhou, E., Zhang, W.*, et al.*
820 (2019). Chemoconnectomics: Mapping Chemical Transmission in Drosophila. Neuron *101*,
821 876-893 e874.
822 Dietrich, M.O., Zimmer, M.R., Bober, J., and Horvath, T.L. (2015). Hypothalamic Agrp
823 neurons drive stereotypic behaviors beyond feeding. Cell *160*, 1222-1232.

824 Dus, M., Lai, J.S., Gunapala, K.M., Min, S., Tayler, T.D., Hergarden, A.C., Geraud, E., Joseph,
825 C.M., and Suh, G.S. (2015). Nutrient Sensor in the Brain Directs the Action of the Brain-Gut
826 Axis in Drosophila. Neuron *87*, 139-151.
827 Fosque, B.F., Sun, Y., Dana, H., Yang, C.T., Ohyama, T., Tadross, M.R., Patel, R., Zlatic, M.,
828 Kim, D.S., Ahrens, M.B.*, et al.* (2015). Neural circuits. Labeling of active neural circuits in vivo
829 with designed calcium integrators. Science *347*, 755-760.
830 Fu, O., Iwai, Y., Narukawa, M., Ishikawa, A.W., Ishii, K.K., Murata, K., Yoshimura, Y.,
831 Touhara, K., Misaka, T., Minokoshi, Y.*, et al.* (2019). Hypothalamic neuronal circuits
832 regulating hunger-induced taste modification. Nat Commun *10*, 4560.
833 Fujii, S., Yavuz, A., Slone, J., Jagge, C., Song, X., and Amrein, H. (2015). Drosophila sugar
834 receptors in sweet taste perception, olfaction, and internal nutrient sensing. Curr Biol *25*, 621-
835 627.
836 Hentze, J.L., Carlsson, M.A., Kondo, S., Nassel, D.R., and Rewitz, K.F. (2015). The
837 Neuropeptide Allatostatin A Regulates Metabolism and Feeding Decisions in Drosophila. Sci
838 Rep *5*, 11680.
839 Hergarden, A.C., Tayler, T.D., and Anderson, D.J. (2012). Allatostatin-A neurons inhibit
840 feeding behavior in adult Drosophila. Proc Natl Acad Sci U S A *109*, 3967-3972.
841 Inagaki, H.K., Ben-Tabou de-Leon, S., Wong, A.M., Jagadish, S., Ishimoto, H., Barnea, G.,
842 Kitamoto, T., Axel, R., and Anderson, D.J. (2012). Visualizing neuromodulation in vivo:
843 TANGO-mapping of dopamine signaling reveals appetite control of sugar sensing. Cell *148*,
844 583-595.
845 Inagaki, H.K., Panse, K.M., and Anderson, D.J. (2014). Independent, reciprocal

846 neuromodulatory control of sweet and bitter taste sensitivity during starvation in Drosophila.
847 Neuron *84*, 806-820.
848 Jin, H., Fishman, Z.H., Ye, M., Wang, L., and Zuker, C.S. (2021). Top-Down Control of Sweet
849 and Bitter Taste in the Mammalian Brain. Cell *184*, 257-271 e216.
850 Karigo, T., and Deutsch, D. (2022). Flexibility of neural circuits regulating mating behaviors in
851 mice and flies. Front Neural Circuits *16*, 949781.
852 Kitamoto, T. (2001). Conditional modification of behavior in Drosophila by targeted expression
853 of a temperature-sensitive shibire allele in defined neurons. J Neurobiol *47*, 81-92.
854 Klapoetke, N.C., Murata, Y., Kim, S.S., Pulver, S.R., Birdsey-Benson, A., Cho, Y.K., Morimoto,
855 T.K., Chuong, A.S., Carpenter, E.J., Tian, Z.*, et al.* (2014). Independent optical excitation of
856 distinct neural populations. Nat Methods *11*, 338-346.
857 Koch, M., Varela, L., Kim, J.G., Kim, J.D., Hernandez-Nuno, F., Simonds, S.E., Castorena,
858 C.M., Vianna, C.R., Elmquist, J.K., Morozov, Y.M.*, et al.* (2015). Hypothalamic POMC
859 neurons promote cannabinoid-induced feeding. Nature *519*, 45-50.
860 Kubrak, O.I., Lushchak, O.V., Zandawala, M., and Nassel, D.R. (2016). Systemic corazonin
861 signalling modulates stress responses and metabolism in Drosophila. Open Biol *6*.
862 Larsen, M.J., Burton, K.J., Zantello, M.R., Smith, V.G., Lowery, D.L., and Kubiak, T.M. (2001).
863 Type A allatostatins from Drosophila melanogaster and Diplotera puncata activate two
864 Drosophila allatostatin receptors, DAR-1 and DAR-2, expressed in CHO cells. Biochem
865 Biophys Res Commun *286*, 895-901.
866 Lin, S., Senapati, B., and Tsao, C.H. (2019). Neural basis of hunger-driven behaviour in
867 Drosophila. Open Biol *9*, 180259.

868 Malita, A., Kubrak, O., Koyama, T., Ahrentlov, N., Texada, M.J., Nagy, S., Halberg, K.V., and
869 Rewitz, K. (2022). A gut-derived hormone suppresses sugar appetite and regulates food
870 choice in Drosophila. Nat Metab *4*, 1532-1550.
871 Marella, S., Mann, K., and Scott, K. (2012). Dopaminergic modulation of sucrose acceptance
872 behavior in Drosophila. Neuron *73*, 941-950.
873 Martelli, C., Pech, U., Kobbenbring, S., Pauls, D., Bahl, B., Sommer, M.V., Pooryasin, A.,
874 Barth, J., Arias, C.W.P., Vassiliou, C.*, et al.* (2017). SIFamide Translates Hunger Signals into
875 Appetitive and Feeding Behavior in Drosophila. Cell Rep *20*, 464-478.
876 Melcher, C., Bader, R., Walther, S., Simakov, O., and Pankratz, M.J. (2006). Neuromedin U
877 and its putative Drosophila homolog hugin. PLoS Biol *4*, e68.
878 Melcher, C., and Pankratz, M.J. (2005). Candidate gustatory interneurons modulating feeding
879 behavior in the Drosophila brain. PLoS Biol *3*, e305.
880 Miroschnikow, A., Schlegel, P., and Pankratz, M.J. (2020). Making Feeding Decisions in the
881 Drosophila Nervous System. Curr Biol *30*, R831-R840.
882 Munch, D., Ezra-Nevo, G., Francisco, A.P., Tastekin, I., and Ribeiro, C. (2020). Nutrient
883 homeostasis - translating internal states to behavior. Curr Opin Neurobiol *60*, 67-75.
884 Oh, Y., Lai, J.S., Mills, H.J., Erdjument-Bromage, H., Giammarinaro, B., Saadipour, K., Wang,
885 J.G., Abu, F., Neubert, T.A., and Suh, G.S.B. (2019). A glucose-sensing neuron pair regulates
886 insulin and glucagon in Drosophila. Nature *574*, 559-564.
887 Oh, Y., Lai, J.S., Min, S., Huang, H.W., Liberles, S.D., Ryoo, H.D., and Suh, G.S.B. (2021).
888 Periphery signals generated by Piezo-mediated stomach stretch and Neuromedin-mediated
889 glucose load regulate the Drosophila brain nutrient sensor. Neuron *109*, 1979-1995 e1976.

890 Park, Y., Kim, Y.J., and Adams, M.E. (2002). Identification of G protein-coupled receptors for
891 Drosophila PRXamide peptides, CCAP, corazonin, and AKH supports a theory of ligand-
892 receptor coevolution. Proc Natl Acad Sci U S A *99*, 11423-11428.
893 Parton, L.E., Ye, C.P., Coppari, R., Enriori, P.J., Choi, B., Zhang, C.Y., Xu, C., Vianna, C.R.,
894 Balthasar, N., Lee, C.E.*, et al.* (2007). Glucose sensing by POMC neurons regulates glucose
895 homeostasis and is impaired in obesity. Nature *449*, 228-232.
896 Qi, W., Wang, G., and Wang, L. (2021). A novel satiety sensor detects circulating glucose and
897 suppresses food consumption via insulin-producing cells in Drosophila. Cell Res *31*, 580-588.
898 Root, C.M., Ko, K.I., Jafari, A., and Wang, J.W. (2011). Presynaptic facilitation by
899 neuropeptide signaling mediates odor-driven food search. Cell *145*, 133-144.
900 Schlegel, P., Texada, M.J., Miroschnikow, A., Schoofs, A., Huckesfeld, S., Peters, M.,
901 Schneider-Mizell, C.M., Lacin, H., Li, F., Fetter, R.D.*, et al.* (2016). Synaptic transmission
902 parallels neuromodulation in a central food-intake circuit. Elife *5*.
903 Schoofs, A., Huckesfeld, S., Schlegel, P., Miroschnikow, A., Peters, M., Zeymer, M., Spiess,
904 R., Chiang, A.S., and Pankratz, M.J. (2014). Selection of motor programs for suppressing
905 food intake and inducing locomotion in the Drosophila brain. PLoS Biol *12*, e1001893.
906 Senapati, B., Tsao, C.H., Juan, Y.A., Chiu, T.H., Wu, C.L., Waddell, S., and Lin, S. (2019). A
907 neural mechanism for deprivation state-specific expression of relevant memories in
908 Drosophila. Nat Neurosci *22*, 2029-2039.
909 Shiraiwa, T., and Carlson, J.R. (2007). Proboscis extension response (PER) assay in
910 Drosophila. J Vis Exp, 193.
911 Song, T., Qin, W., Lai, Z., Li, H., Li, D., Wang, B., Deng, W., Wang, T., Wang, L., and Huang,

912 R. (2023). Dietary cysteine drives body fat loss via FMRFamide signaling in Drosophila and
913 mouse. Cell Res *33*, 434-447.
914 Stocker, R.F. (2004). Taste perception: Drosophila - a model of good taste. Curr Biol *14*,
915 R560-561.
916 Sun, J., Liu, C., Bai, X., Li, X., Li, J., Zhang, Z., Zhang, Y., Guo, J., and Li, Y. (2017).
917 Drosophila FIT is a protein-specific satiety hormone essential for feeding control. Nat
918 Commun *8*, 14161.
919 Sun, M., Ma, M., Deng, B., Li, N., Peng, Q., and Pan, Y. (2023). A neural pathway underlying
920 hunger modulation of sexual receptivity in Drosophila females. Cell Rep *42*, 113243.
921 Teranishi, H., and Hanada, R. (2021). Neuromedin U, a Key Molecule in Metabolic Disorders.
922 Int J Mol Sci *22*.
923 Ugrankar, R., Theodoropoulos, P., Akdemir, F., Henne, W.M., and Graff, J.M. (2018).
924 Circulating glucose levels inversely correlate with Drosophila larval feeding through insulin
925 signaling and SLC5A11. Commun Biol *1*, 110.
926 Vivot, K., Meszaros, G., Pangou, E., Zhang, Z., Qu, M., Erbs, E., Yeghiazaryan, G., Quinones,
927 M., Grandgirard, E., Schneider, A.*, et al.* (2023). CaMK1D signalling in AgRP neurons
928 promotes ghrelin-mediated food intake. Nat Metab *5*, 1045-1058.
929 Wang, M., Wu, J.X., Ding, D., and Chen, L. (2022). Structural insights into the mechanism of
930 pancreatic K(ATP) channel regulation by nucleotides. Nat Commun *13*, 2770.
931 Wei, Q., Krolewski, D.M., Moore, S., Kumar, V., Li, F., Martin, B., Tomer, R., Murphy, G.G.,
932 Deisseroth, K., Watson, S.J., Jr.*, et al.* (2018). Uneven balance of power between
933 hypothalamic peptidergic neurons in the control of feeding. Proc Natl Acad Sci U S A *115*,

934 E9489-E9498.

935 Willyard, C. (2008). Hungry for sleep. Nat Med *14*, 477-480.

936 Yao, Z., and Scott, K. (2022). Serotonergic neurons translate taste detection into internal
937 nutrient regulation. Neuron *110*, 1036-1050 e1037.

938 Yarmolinsky, D.A., Zuker, C.S., and Ryba, N.J. (2009). Common sense about taste: from
939 mammals to insects. Cell *139*, 234-244.

940 Yoon, N.A., and Diano, S. (2021). Hypothalamic glucose-sensing mechanisms. Diabetologia
941 *64*, 985-993.

942 Yu, Y., Huang, R., Ye, J., Zhang, V., Wu, C., Cheng, G., Jia, J., and Wang, L. (2016).
943 Regulation of starvation-induced hyperactivity by insulin and glucagon signaling in adult
944 Drosophila. Elife *5*.

945 Yurgel, M.E., Kakad, P., Zandawala, M., Nassel, D.R., Godenschwege, T.A., and Keene, A.C.
946 (2019). A single pair of leucokinin neurons are modulated by feeding state and regulate sleep-
947 metabolism interactions. PLoS Biol *17*, e2006409.

948 Zhao, Y., Khallaf, M.A., Johansson, E., Dzaki, N., Bhat, S., Alfredsson, J., Duan, J., Hansson,
949 B.S., Knaden, M., and Alenius, M. (2022). Hedgehog-mediated gut-taste neuron axis controls
950 sweet perception in Drosophila. Nat Commun *13*, 7810.

951

952

Figure legends

Figure 1. hugin^{+} neurons were a novel glucose sensor in the fly brain.

(**A**) Experimental procedure schematic. Newly eclosed flies were gathered and provided with regular food for 5 days, followed by a 24-hour period of starvation. Proboscis Extension Response (PER) assays were conducted. (**B**) Fraction of flies showing PER to different concentrations of sucrose (n=4 groups, each of 10 flies). (**C-D**) Fraction of flies of the indicated genotypes under 30 ºC showing PER to 400 mM of sucrose (n=4-5 groups, each of 10 flies). (**E**) Fraction of indicated flies showing PER to different concentrations of sucrose (ND represent standard fly food) (n=4-5 groups, each of 10 flies). (**F**) hugin expression in the brain, illustrated by mCD8::GFP expression driven by *hugin^{GAL4}*. Scale bar represents 100 μm. (**G**) Representative traces and quantification of ex vivo calcium responses of hugin^{+} neurons during the perfusion of glucose with or without TTX (n=6-7). Horizontal black bar represents the duration indicated glucose solution stimulation. (**H**) AstA expression in the brain, illustrated by mCD8::GFP expression driven by *AstA^{GAL4}*. Scale bar represents 100 μm. (**I**) Representative traces and quantification of ex vivo calcium responses of AstA^{+} neurons during the perfusion of glucose with or without TTX (n=6). (**J**) Representative images of pre-photoconversion (pre-PC) and post-photoconversion (post-PC) CaMPARI signal in hugin-expressing neurons (upper). The Red:Green ratio represents intracellular Ca^{2+} concentrations (lower). Scale bar represents 100 μm (n=18-23). ns, $P > 0.05$; *$P < 0.05$; **$P < 0.01$; ***$P < 0.001$; ****$P < 0.0001$. Student's *t-test*, one-way and two-way ANOVA followed by post hoc test with Bonferroni correction were used for multiple comparisons when applicable.

Figure 2. Glucose activated hugin$^+$ neurons via Gltu1 and K_{ATP} channel.

(**A**) Representative traces and quantification of ex vivo calcium responses of hugin$^+$ neurons during the perfusion of glucose with or without phlorizin (1mM, n=6-7). Horizontal black bar represents the duration indicated glucose solution stimulation. (**B**) Representative traces and quantification of ex vivo calcium responses of hugin$^+$ neurons in indicated flies during the perfusion of glucose. (**C**) Fraction of flies of the indicated genotypes showing PER to different concentrations of sucrose (n=4 groups, each of 10 flies). (**D-E**) Representative traces and quantification of ex vivo calcium responses of hugin$^+$ neurons during the perfusion of glibenclamide (100 μM, D), glucose with alloxan (10 μM, E). (**F**) Representative traces and quantification of ex vivo calcium responses of hugin$^+$ neurons in indicated flies during the perfusion of glucose. (**G**) Representative traces and quantification of ex vivo calcium responses of hugin$^+$ neurons during the perfusion of pyruvate (50 mM, n=6). (**H**) Representative traces and quantification of ex vivo calcium responses of hugin$^+$ neurons during the perfusion of D-glucose and L-glucose (50 mM, n=6) ns, $P > 0.05$; *$P < 0.05$; **$P < 0.01$; ****$P < 0.0001$. Student's t-test and two-way ANOVA followed by post hoc test with Bonferroni correction were used for multiple comparisons when applicable.

Figure 3. hugin$^+$ neurons activated AstA$^+$ neurons through PK2-R1.

(**A**) Fraction of flies showing PER to different concentrations of sucrose (n=4 groups, each of 10 flies). Flies were injected with saline or synthetic hugin for 30 minutes before the assay. (**B**) Representative traces (upper) and quantification (lower) of peak calcium transients of Gr5a$^+$ neurons in indicated flies upon 5% sucrose after injection of synthetic hugin (n=6). Horizontal black bar represents the duration sucrose stimulation. (**C-D**) Fraction of flies of the indicated genotypes showing PER to different concentrations of sucrose (n=4 groups, each of 10 flies). (**E**) Co-localization (dashed box) of PK2-R1$^+$ neurons (green) and AstA$^+$ neurons (red) in the SEZ region. Scale bar represents 100 μm. (**F**) Representative traces (upper) and quantification (lower) of peak calcium transients of AstA$^+$ neurons after the photo-activation of hugin$^+$ neurons (n=6) from in vivo calcium imaging. Horizontal black bar represents the duration of red-light stimulation. (**G-H**) Fraction of flies of the indicated genotypes showing PER to different concentrations of sucrose (n=4 groups, each of 10 flies). ns, $P > 0.05$; *$P < 0.05$; **$P < 0.01$; ***$P < 0.001$; ****$P < 0.0001$. Student's *t-test* and two-way ANOVA followed by post hoc test with Bonferroni correction were used for multiple comparisons when applicable.

Figure 4. AstA$^+$ neurons inhibited Gr5a$^+$ neurons through AstA-R1.

(**A**) Fraction of flies showing PER to different concentrations of sucrose (n=4 groups, each of 10 flies). Flies were injected with saline or synthetic AstA for 30 minutes before the assay. (**B**) Representative traces (left) and quantification (right) of peak calcium transients of Gr5a$^+$ neurons in indicated flies upon 5% sucrose after injection of synthetic AstA (n=6). Horizontal black bar represents the duration sucrose stimulation. (**C**) Localization of Gr5a$^+$ neurons (green) and AstA$^+$ neurons (red) in the brain. Scale bar represents 100 μm. (**D**) Co-localization of Gr5a$^+$ neurons (green) and AstA-R1$^+$ neurons (red). Arrows point to the neurons co-expressing the two receptors. Scale bar represents 50 μm. (**E-F**) Fraction of flies of the indicated genotypes showing PER to different concentrations of sucrose (n=4 groups, each of 10 flies). (**G-H**) Representative traces (left) and quantification (right) of peak calcium transients of Gr5a$^+$ neurons in indicated flies upon 5% sucrose during the process of photo-activation of AstA$^+$ neurons (G, n=6) and hugin$^+$ neurons (H, n=7-8). Shadows represents the duration of red-light stimulation. Horizontal black bar represents the duration of sucrose stimulation. ns, $P > 0.05$; *$P < 0.05$; ***$P < 0.001$; ****$P < 0.0001$. Student's *t-test* and two-way ANOVA followed by post hoc test with Bonferroni correction were used for multiple comparisons when applicable.

Figure 5. NMU^+ neurons were the central energy sensor in mouse.

(**A**) Blood NMU levels of starved mice re-fed with 20% sucrose (n=6). (**B**) Two-bottle preference tests for starved mice re-fed with sucrose (n=7). (**C**) Two-bottle preference tests for starved mice with or without intraperitoneal injection of NMU peptide (YFLFRPRN-NH_2, 4.5μm/kg) (n=7). (**D**) Two-bottle preference tests for indicated starved mice. (**E**) Fiber photometry to record the calcium dynamics of NMU^+ neurons in the VMH with GCaMP6m. (**F-G**) Representative trace (left) and heatmaps (right, n=5) showing calcium dynamics of NMU^+ neurons in the VMH in response to glucose perfusion. (**H**) Experimental approach to assess calcium signaling in NMU^+ neurons in the VMH in vitro. (**I-J**) Representative traces and quantification of ex vivo calcium responses of NMU^+ neurons during the perfusion of glucose with or without TTX (I), Alloxan (J) and Phlorizin (J) (n=6-7). Horizontal black bar represents the duration indicated glucose solution stimulation. (**K**) Anterograde tracing the downstream terget of NMU neurons. (**L**) Fiber photometry to record the calcium dynamics of $Calb2^+$ neurons in the rNST with GCaMP6m. (**M**) Representative traces and quantification of calcium responses of $Calb2^+$ neurons during glucose feeding with or without NMU injection. ns, $P > 0.05$; *$P < 0.05$; **$P < 0.01$; ***$P < 0.001$; ****$P < 0.0001$. Student's *t-test* and one-way ANOVA followed by post hoc test with Bonferroni correction was used for multiple comparisons when applicable.

Figure supplementary 1. Satiety suppressed sweet sensitivity in a dopamine-independent manner.

(**A**) Representative traces (left) and quantification (right) of peak calcium transients of $Gr5a^+$ neurons in indicated flies (n=6). Horizontal black bar represents the duration 5% sucrose stimulation. (**B-D**) Fraction of flies of the indicated genotypes showing PER to different concentrations of sucrose (B-C, n=4 groups, each of 10 flies). The Area Under the Curve (AUC, D) represents sweet sensitivity in C. *P < 0.05; ****P < 0.0001. Student's *t-test* and two-way ANOVA followed by post hoc test with Bonferroni correction were used for multiple comparisons when applicable.

Figure supplementary 2. The effect of satiety signals on taste modulation.

(**A**) Fraction of fed flies of the indicated genotypes and environmental temperatures showing PER to different concentrations of sucrose (n=4 groups, each of 10 flies). (**B**) Fraction of starved flies of the indicated genotypes and environmental temperatures showing PER to different concentrations of sucrose (n=4-5 groups, each of 10 flies). ns, P > 0.05; *P < 0.05; ***P < 0.001; ****P < 0.0001. Two-way ANOVA followed by post hoc test with Bonferroni correction was used for multiple comparisons when applicable.

Figure supplementary 3. Activation of IPCs decreased the circulating sugar levels and increased sweet sensitivity.

(**A**) Hemolymph glucose levels from the indicated genotypes and treatment temperatures (n=8-9, 1 hour at 30 ºC). (**B-C**) Fraction of fed flies of the indicated genotypes and

environmental temperatures showing PER to different concentrations of sucrose (n=4 groups, each of 10 flies). ns, P > 0.05; ****P < 0.0001. Student's *t-test* and two-way ANOVA followed by post hoc test with Bonferroni correction were used for multiple comparisons when applicable.

Figure supplementary 4. Sugar intake suppressed sweet sensation.

(**A**) Fraction of indicated flies showing PER to different concentrations of fructose (n=4 groups, each of 10 flies). (**B**) Fraction of indicated flies showing PER to different concentrations of trehalose (n=4 groups, each of 10 flies).****P < 0.0001. two-way ANOVA followed by post hoc test with Bonferroni correction were used for multiple comparisons when applicable.

Figure supplementary 5. Starvation led to a decrease in the circulating sugar levels.

Hemolymph glucose levels from indicated flies (n=6-8). ***P < 0.001. Student's *t-test* was used for comparisons.

Figure supplementary 6. The response of different neuropeptide-expressing neurons to glucose.

(**A**) LK expression in the brain, illustrated by mCD8::GFP expression driven by LK^{GAL4}. Scale bar represents 100 μm. (**B**) Representative traces and quantification of ex vivo calcium responses of LK^{+} neurons during the perfusion of glucose (n=6). (**C-D**) The distribution (C) and calcium responses (D) of TK^{+} neurons (n=6). (**E-F**) The distribution (E) and calcium

responses (F) of CCHa1^{+} neurons (n=6). (**G-H**) The distribution (G) and calcium responses (H) of CCHa2^{+} neurons (n=6).

Figure supplementary 7. The calcium response of hugin neurons upon glucose stimuli.

(**A**) Representative image of hugin neurons in SEZ. Scale bar represents 50 μm. (**B**) Calcium responses of different cluster of hugin neurons during the prefusion of glucose (n=6)..*P < 0.05; ***P < 0.001. Student's *t-test* used for comparisons.

Figure supplementary 8. hugin^{+} or AstA^{+} neurons suppressed sweet taste.

(**A-D**) Fraction of flies of the indicated genotypes and environmental temperatures showing PER to different concentrations of sucrose (n=4-5 groups, each of 10 flies). ns, P > 0.05; *P < 0.05; ***P < 0.001; ****P < 0.0001. Two-way ANOVA followed by post hoc test with Bonferroni correction was used for multiple comparisons when applicable.

Figure supplementary 9. The calcium response of AstA^{+} neurons upon glucose treatment.

(**A**) Representative image of different part of AstA neurons .Scale bar represents 50 μm. (**B**) Calcium responses of different cluster of hugin neurons during the prefusion of glucose (n=6)

Figure supplementary 10. Knockout of *PK2-R1* enhanced sweet sensation.

(**A-C**) Fraction of flies of the indicated genotypes showing PER to different concentrations of sucrose (n=4 groups, each of 10 flies). ***P < 0.001; ****P < 0.0001. Two-way ANOVA followed by post hoc test with Bonferroni correction were used for multiple comparisons

when applicable.

Figure supplementary 11. hugin^{+} neurons in the brain activated AstA^{+} neurons. (**A-B**) Fraction of flies of the indicated genotypes and environmental temperatures showing PER to different concentrations of sucrose (n=4 groups, each of 10 flies). Note connection between the brain and VNC was cut off before the behavioral assay. (**C**) Representative traces (upper) and quantification (lower) of peak calcium transients of AstA^{+} neurons after the photo-activation of hugin^{+} neurons (n=6) from ex vivo calcium imaging. Horizontal black bar represents the duration of red-light stimulation.

Figure supplementary 12. Manipulating gene *AstA-R1* enhance PER.

(**A-C**) Fraction of flies of the indicated genotypes showing PER to different concentrations of sucrose (n=4 groups, each of 10 flies). ***P < 0.001; ****P < 0.0001. Two-way ANOVA followed by post hoc test with Bonferroni correction were used for multiple comparisons when applicable.

Figure supplementary 13. hugin-AstA-Gr5a circuitry inhibited feeding behavior.

(**A**) The illustration of experimental design in Figure supplementary 13B-C. Note that all flies were maintained at 20ºC before the feeding assay to prevent neuronal silencing by Shibire^{ts1} during these procedures. (**B-C**) Food consumption of flies of the indicated genotypes and environmental temperatures (n=8 groups, each of 4 flies). (**D**) Food consumption of flies of the indicated genotypes (n=8 groups, each of 4 flies). (**E**) The TG

content of indicated genotypes (n=8 groups, each of 2 flies). (**F**) Food consumption of flies of the indicated genotypes (n=8 groups, each of 4 flies). ns, P > 0.05; ***P < 0.001; ****P < 0.0001. Student's *t-test* and two-way ANOVA followed by post hoc test with Bonferroni correction were used for multiple comparisons when applicable.

Figure supplementary 14. NMU peptide suppressed sweet taste in fly.

Fraction of flies showing PER to different concentrations of sucrose (n=4 groups, each of 10 flies). Flies were injected with saline or synthetic NMU for 30 mins before the assay.**P < 0.01; ****P < 0.0001. Two-way ANOVA followed by post hoc test with Bonferroni correction were used for multiple comparisons when applicable.

Figure supplementary 15. The expressing pattern of NMU neurons and Calb2 neurons(**A**) Co-labeling of NMU^{+} neurons using a Cre-dependent mCherry reporter (red) and in situ hybridization (green).Scale bar represents 200 μm. (**B**) NMU arbors was extended near $Calb2^{rNST}$ neurons. Scale bar represents 200 μm. (**C**) Co-labeling of $Calb2^{+}$ neurons with a Cre-dependent mCherry reporter (red) and NMU antiboy staining (green). Scale bar represents 200 μm.

Figure supplementary 16. A working model

In the fly brain, a small group of neurons expressing hugin peptide is responsible for detecting the circulating glucose levels. Following feeding, as the levels of glucose in the circulatory system increased, these neurons are activated, leading to the release of hugin, which activated

1156 AstA neurons via its receptor PK2-R1. Subsequently, the activation of $AstA^+$ neurons then
1157 directly inhibited sweet perception via AstA peptide and its cognate receptor AstA-R1
1158 expressed in sweet-sensing $Gr5a^+$ neurons. This neural circuitry is a novel energy sensor that
1159 suppressed sweet perception and terminated feeding behavior, providing an efficient
1160 mechanism for maintaining energy homeostasis.
1161
1162
1163

Figure 1

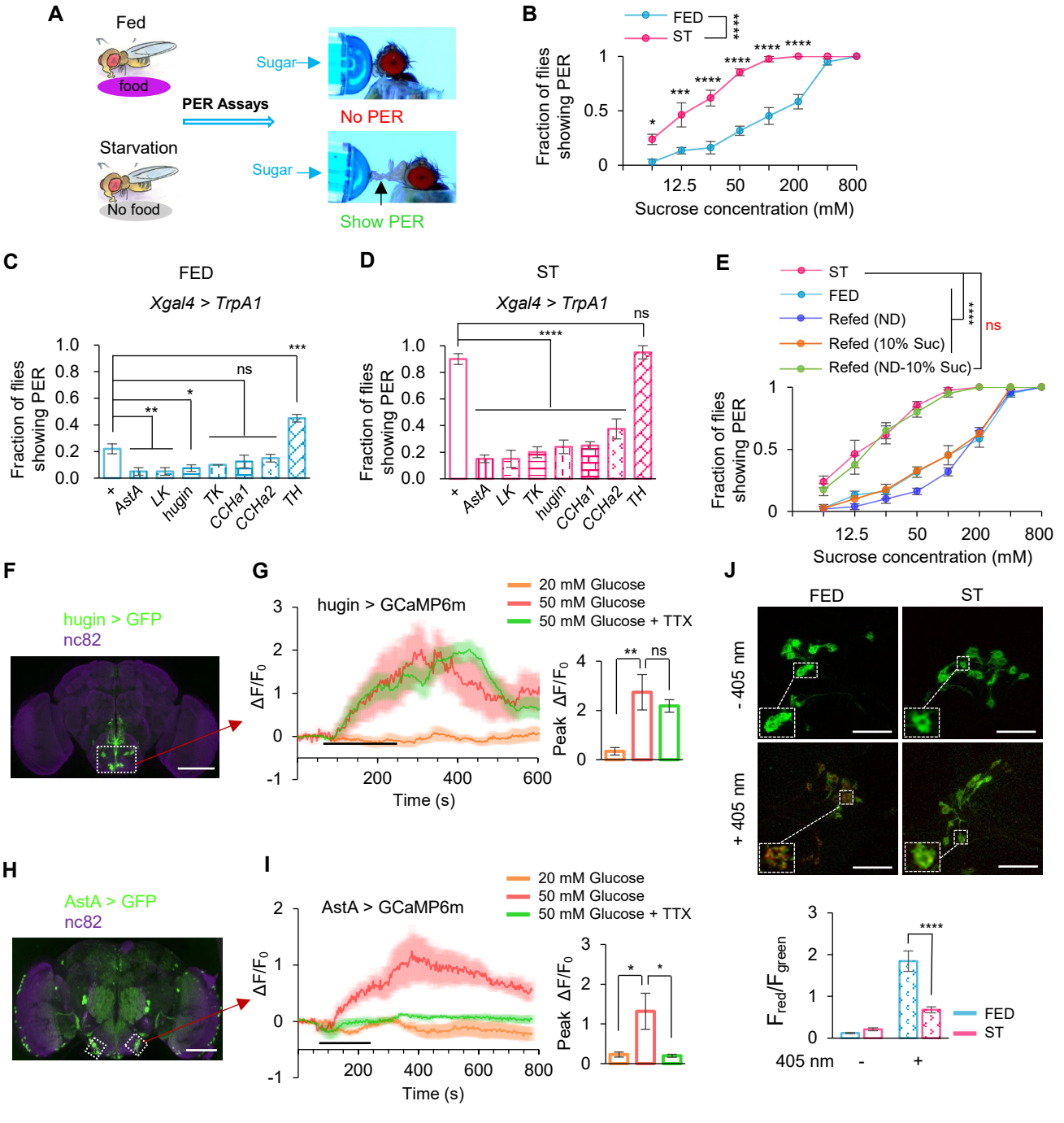
A
Fed
food
Sugar
PER Assays
No PER
Starvation
No food
Sugar
Show PER
B
FED
ST
Fraction of flies showing PER
Sucrose concentration (mM)
C
FED
Xgal4 > TrpA1
Fraction of flies showing PER
+
AstA
LK
hugin
TK
CCHa1
CCHa2
TH
D
ST
Xgal4 > TrpA1
E
ST
FED
Refed (ND)
Refed (10% Suc)
Refed (ND-10% Suc)
F
hugin > GFP
nc82
G
hugin > GCaMP6m
20 mM Glucose
50 mM Glucose
50 mM Glucose + TTX
ΔF/F0
Time (s)
Peak ΔF/F0
J
FED
ST
- 405 nm
+ 405 nm
Fred/Fgreen
405 nm
H
AstA > GFP
nc82
I
AstA > GCaMP6m

Figure 2

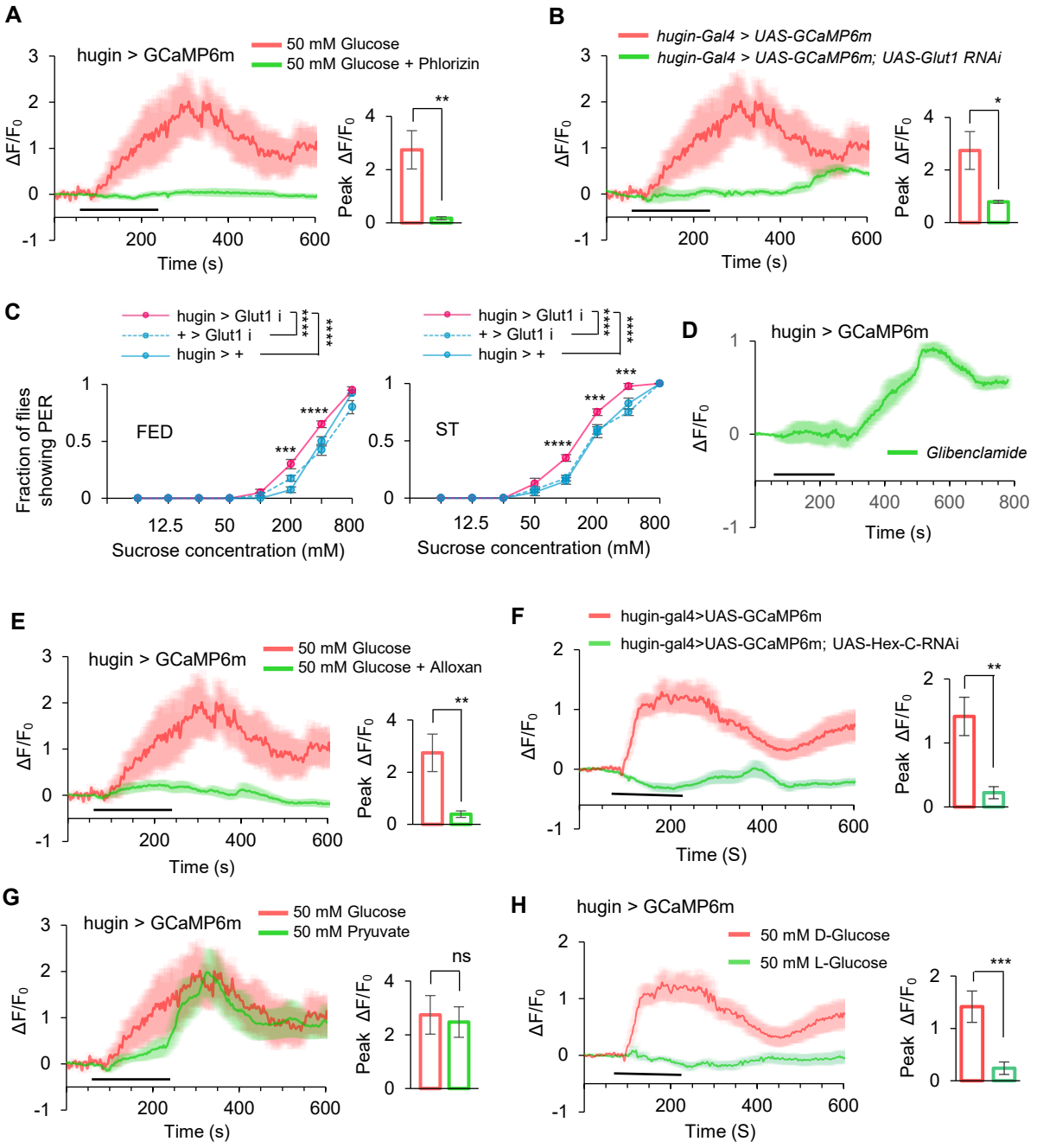
A
hugin > GCaMP6m
50 mM Glucose
50 mM Glucose + Phlorizin
ΔF/F0
Time (s)
Peak ΔF/F0
**
B
hugin-Gal4 > UAS-GCaMP6m
hugin-Gal4 > UAS-GCaMP6m; UAS-Glut1 RNAi
ΔF/F0
Time (s)
Peak ΔF/F0
*
C
hugin > Glut1 i
+ > Glut1 i
hugin > +
****
FED
ST
Fraction of flies showing PER
Sucrose concentration (mM)
12.5
50
200
800
***
D
hugin > GCaMP6m
Glibenclamide
ΔF/F0
Time (s)
E
hugin > GCaMP6m
50 mM Glucose
50 mM Glucose + Alloxan
ΔF/F0
Time (s)
Peak ΔF/F0
**
F
hugin-gal4>UAS-GCaMP6m
hugin-gal4>UAS-GCaMP6m; UAS-Hex-C-RNAi
ΔF/F0
Time (S)
Peak ΔF/F0
**
G
hugin > GCaMP6m
50 mM Glucose
50 mM Pryuvate
ΔF/F0
Time (s)
Peak ΔF/F0
ns
H
hugin > GCaMP6m
50 mM D-Glucose
50 mM L-Glucose
ΔF/F0
Time (S)
Peak ΔF/F0
***

Figure 3

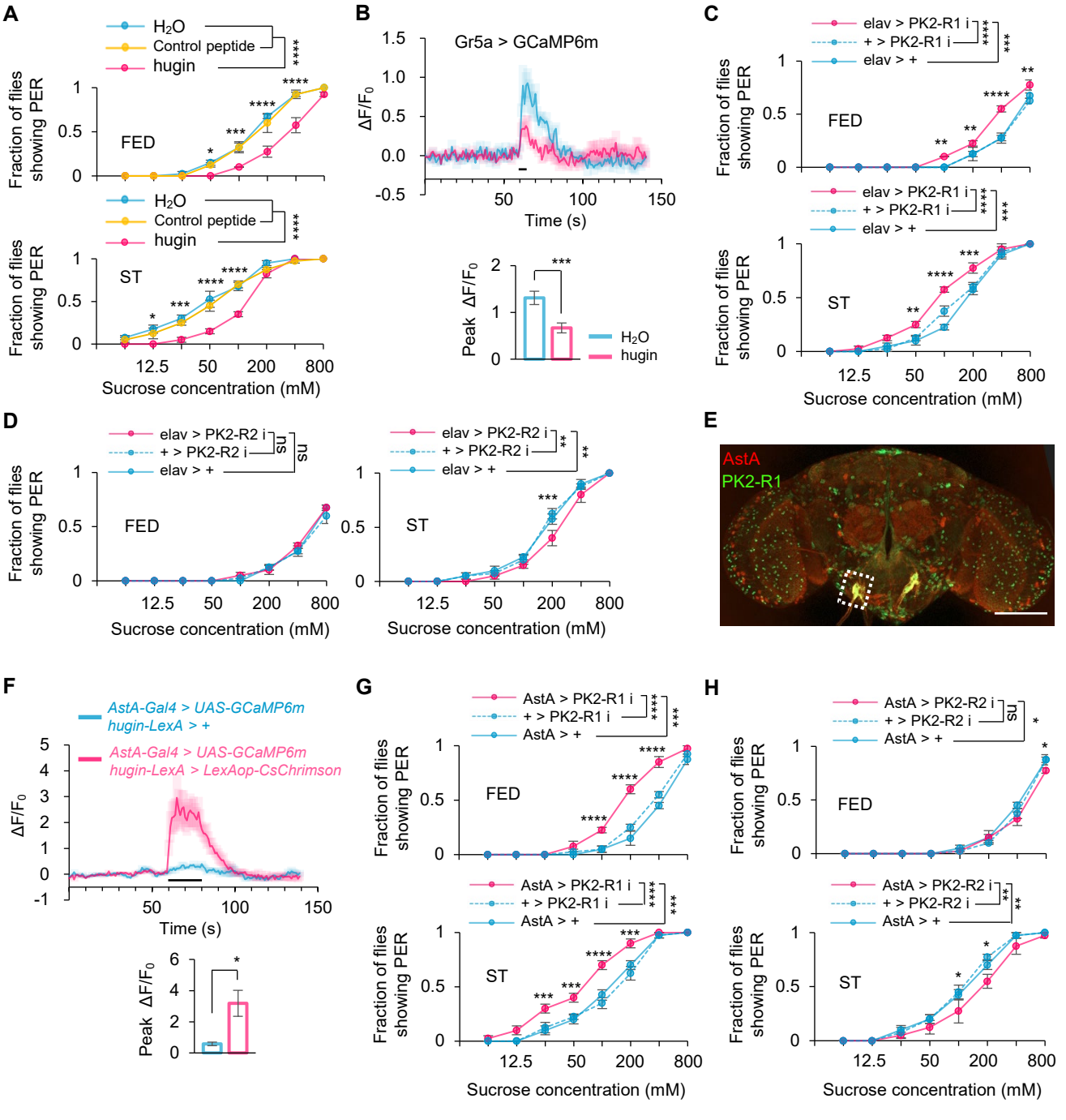
A
H2O
Control peptide
hugin
Fraction of flies showing PER
FED
ST
Sucrose concentration (mM)
B
Gr5a > GCaMP6m
ΔF/F0
Time (s)
Peak ΔF/F0
H2O
hugin
C
elav > PK2-R1 i
+ > PK2-R1 i
elav > +
D
elav > PK2-R2 i
+ > PK2-R2 i
ns
E
AstA
PK2-R1
F
AstA-Gal4 > UAS-GCaMP6m
hugin-LexA > +
AstA-Gal4 > UAS-GCaMP6m
hugin-LexA > LexAop-CsChrimson
G
AstA > PK2-R1 i
+ > PK2-R1 i
AstA > +
H
AstA > PK2-R2 i
+ > PK2-R2 i

Figure 4

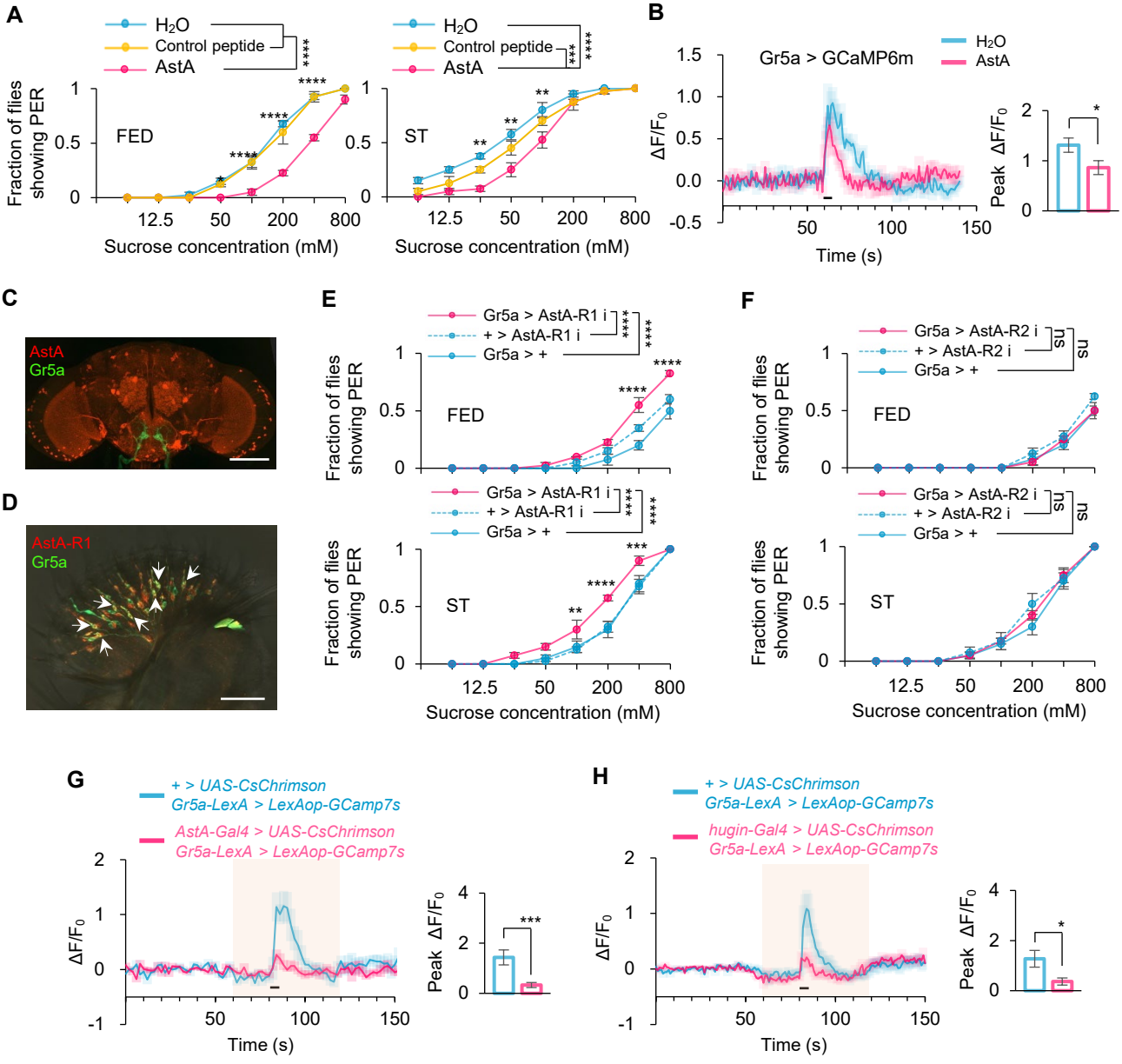
A
H2O
Control peptide
AstA
Fraction of flies showing PER
FED
ST
Sucrose concentration (mM)
B
Gr5a > GCaMP6m
H2O
AstA
ΔF/F0
Time (s)
Peak ΔF/F0
C
AstA
Gr5a
D
AstA-R1
Gr5a
E
Gr5a > AstA-R1 i
+ > AstA-R1 i
Gr5a > +
F
Gr5a > AstA-R2 i
+ > AstA-R2 i
Gr5a > +
ns
G
+ > UAS-CsChrimson
Gr5a-LexA > LexAop-GCamp7s
AstA-Gal4 > UAS-CsChrimson
Gr5a-LexA > LexAop-GCamp7s
H
+ > UAS-CsChrimson
Gr5a-LexA > LexAop-GCamp7s
hugin-Gal4 > UAS-CsChrimson
Gr5a-LexA > LexAop-GCamp7s

Figure 5

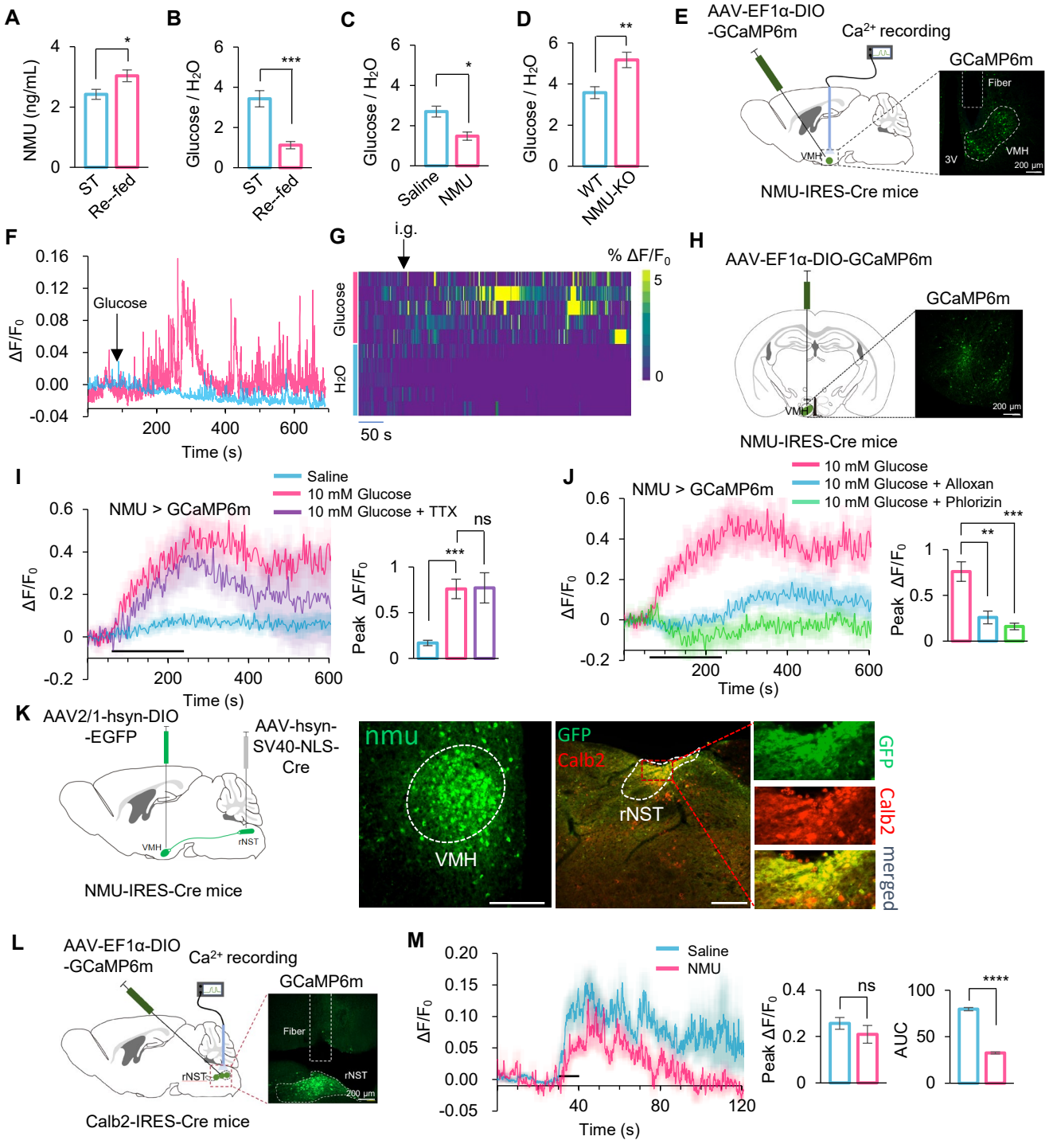
A
NMU (ng/mL)
ST
Re-fed
B
Glucose / H2O
ST
Re-fed
C
Glucose / H2O
Saline
NMU
D
Glucose / H2O
WT
NMU-KO
E
AAV-EF1α-DIO -GCaMP6m
Ca2+ recording
GCaMP6m
Fiber
VMH
3V
200 μm
NMU-IRES-Cre mice
F
Glucose
ΔF/F0
Time (s)
G
i.g.
% ΔF/F0
Glucose
H2O
50 s
H
AAV-EF1α-DIO-GCaMP6m
GCaMP6m
VMH
200 μm
NMU-IRES-Cre mice
I
Saline
10 mM Glucose
10 mM Glucose + TTX
NMU > GCaMP6m
ΔF/F0
Time (s)
Peak ΔF/F0
ns
J
10 mM Glucose
10 mM Glucose + Alloxan
10 mM Glucose + Phlorizin
NMU > GCaMP6m
ΔF/F0
Time (s)
Peak ΔF/F0
K
AAV2/1-hsyn-DIO -EGFP
AAV-hsyn-SV40-NLS-Cre
VMH
rNST
NMU-IRES-Cre mice
nmu
VMH
GFP
Calb2
rNST
GFP
Calb2
merged
L
AAV-EF1α-DIO -GCaMP6m
Ca2+ recording
GCaMP6m
Fiber
rNST
200 μm
Calb2-IRES-Cre mice
M
Saline
NMU
ΔF/F0
Time (s)
Peak ΔF/F0
ns
AUC

Figure supplementary 1

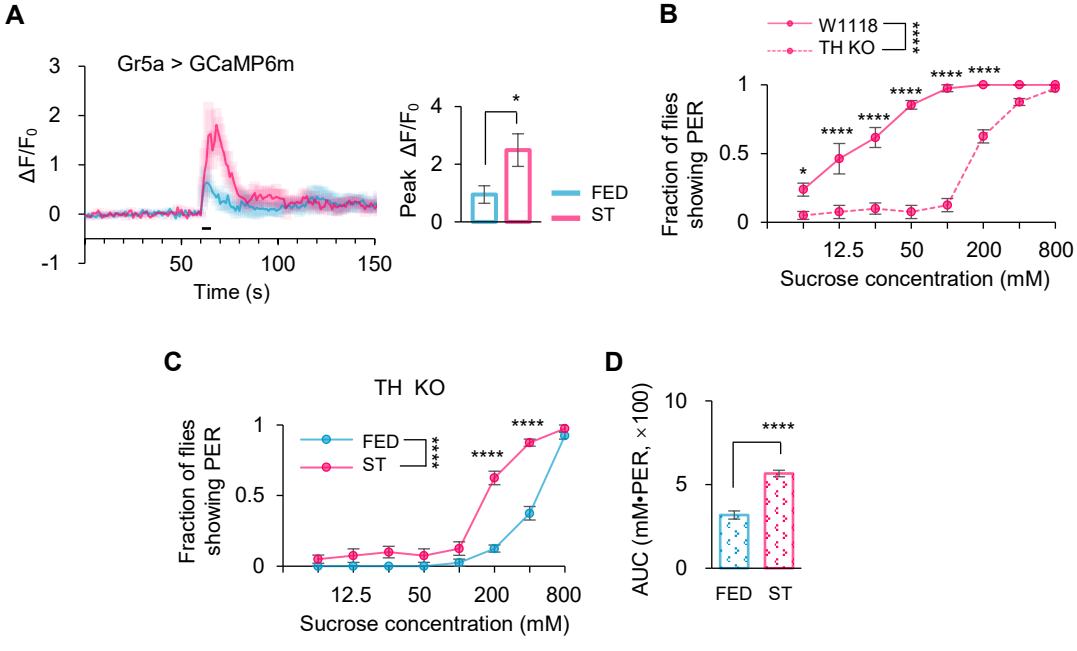

Figure supplementary 2

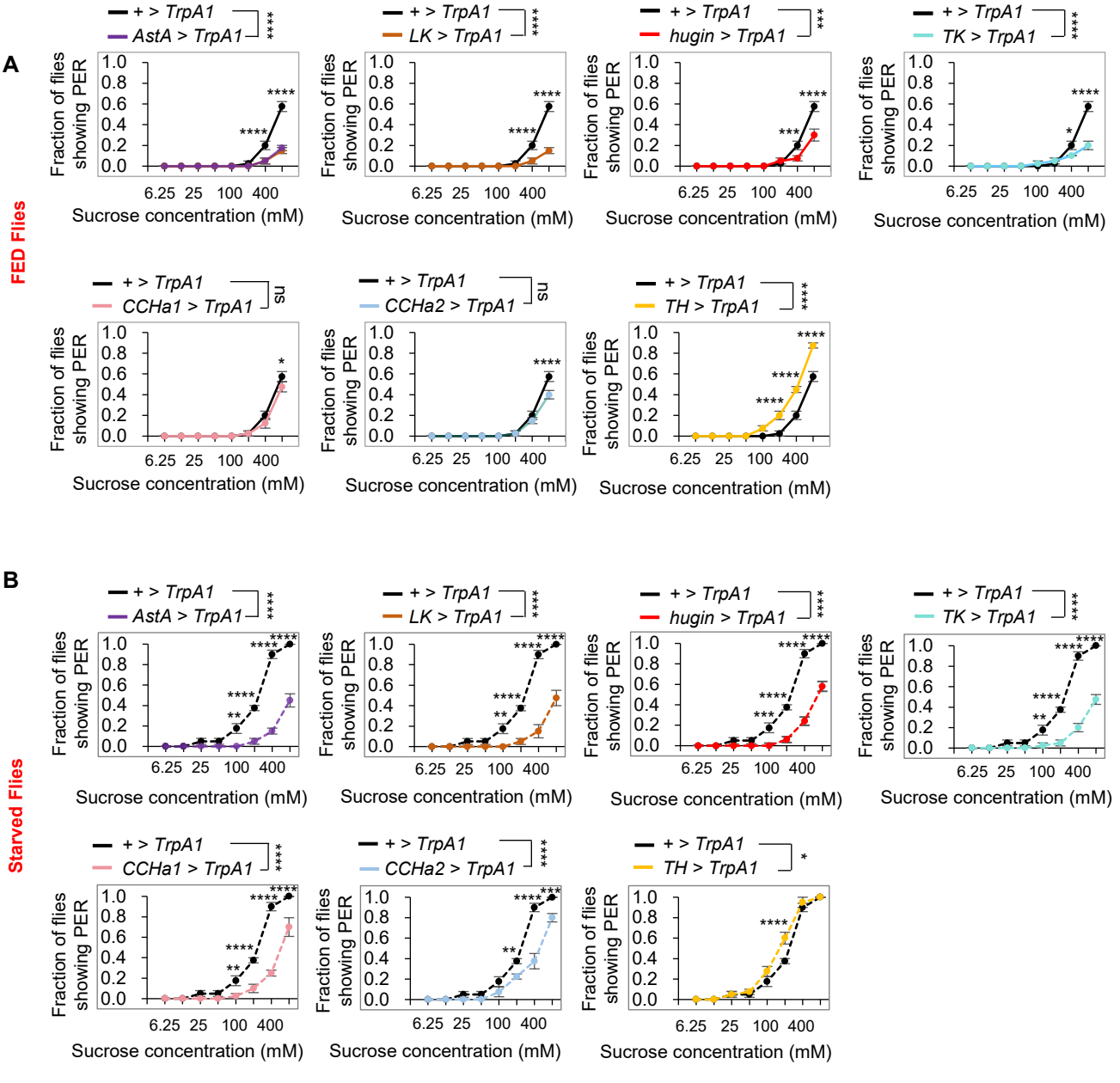

Figure supplementary 3

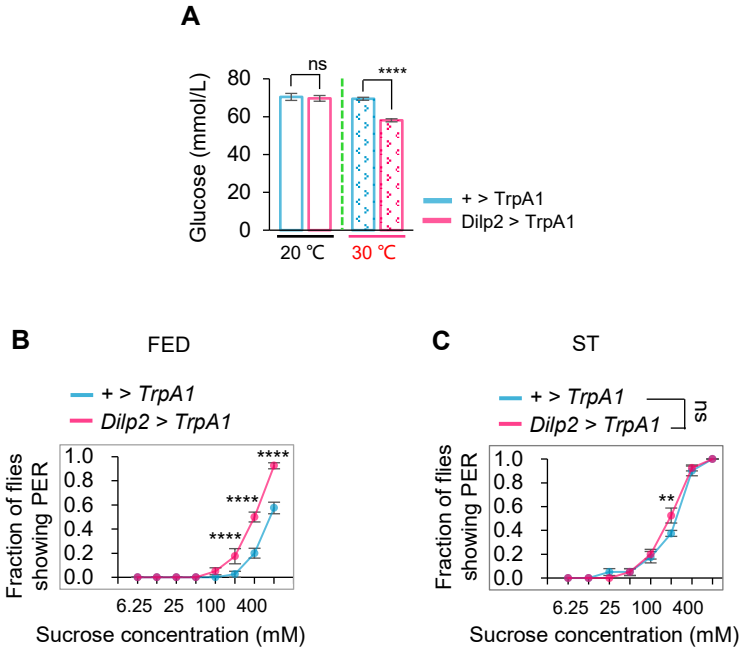

Figure supplementary 4

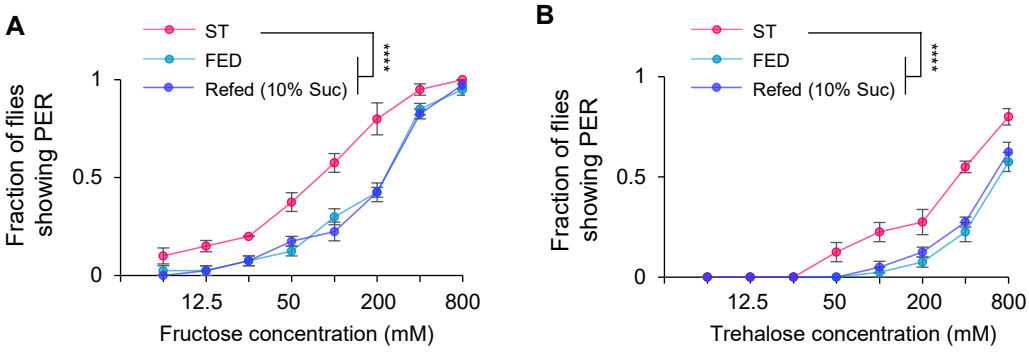

Figure supplementary 5

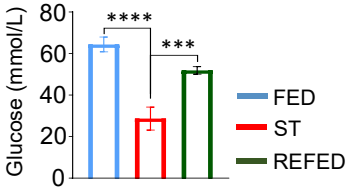

Figure supplementary 6

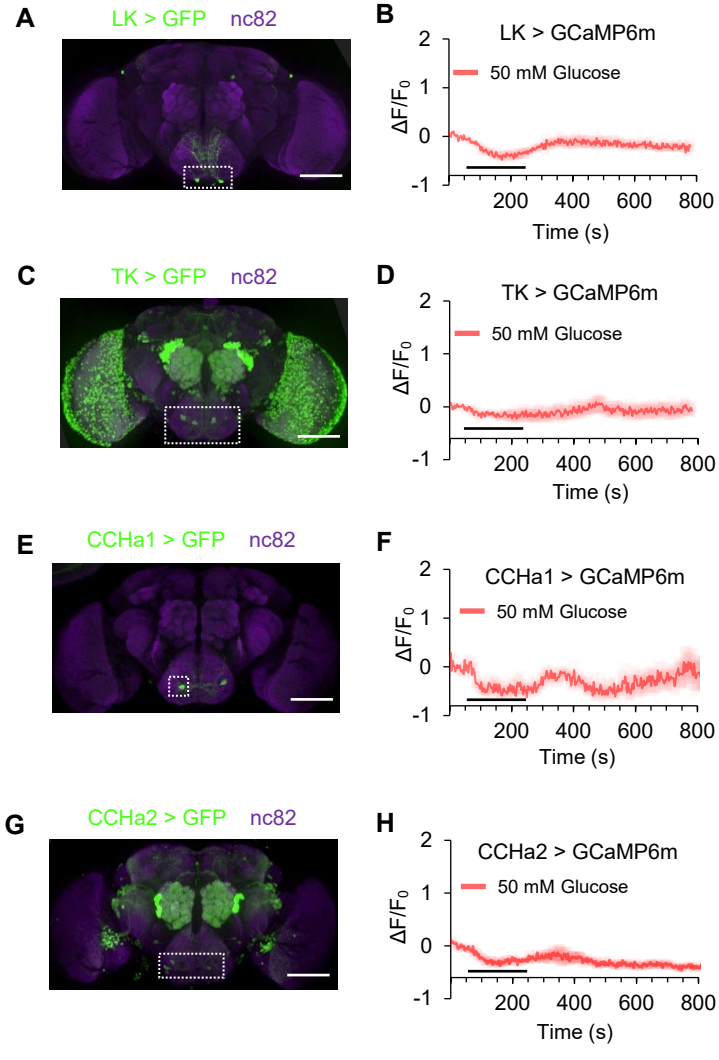

Figure supplementary 7

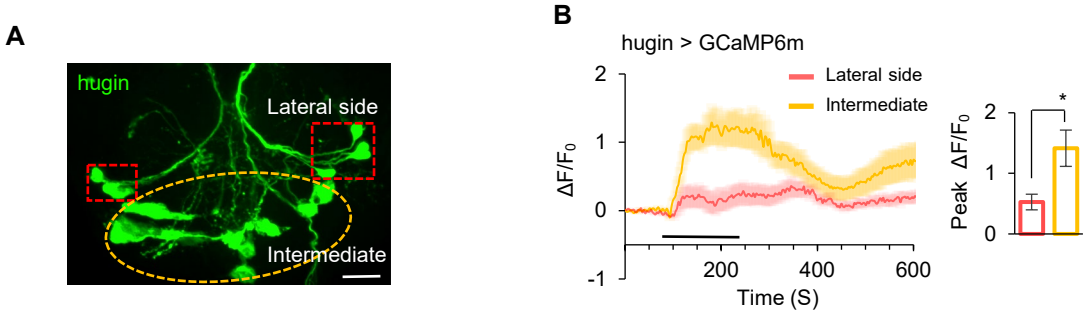

Figure supplementary 8

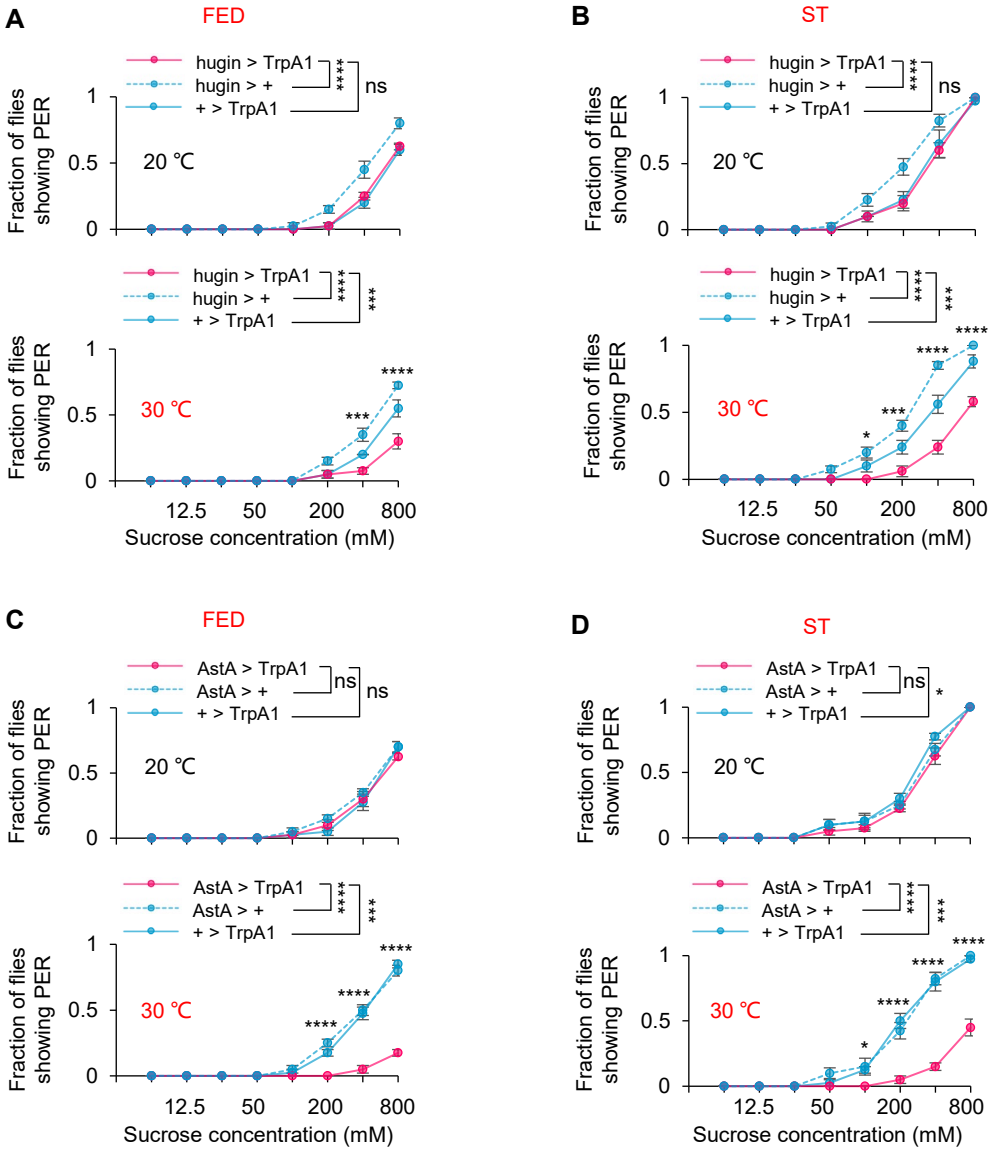

Figure supplementary 9

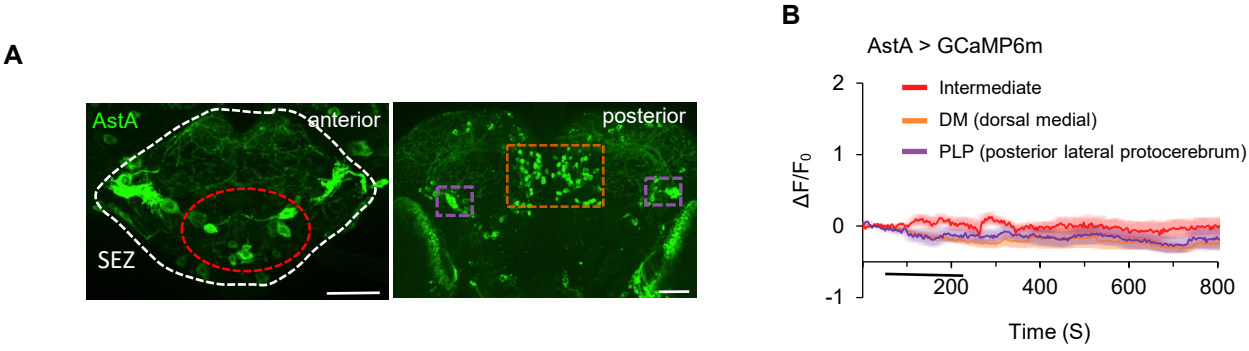

Figure supplementary 10

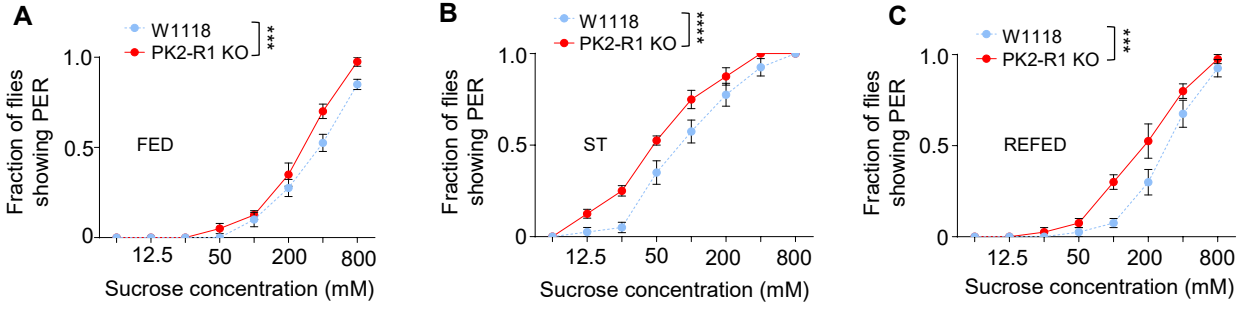

Figure supplementary 11

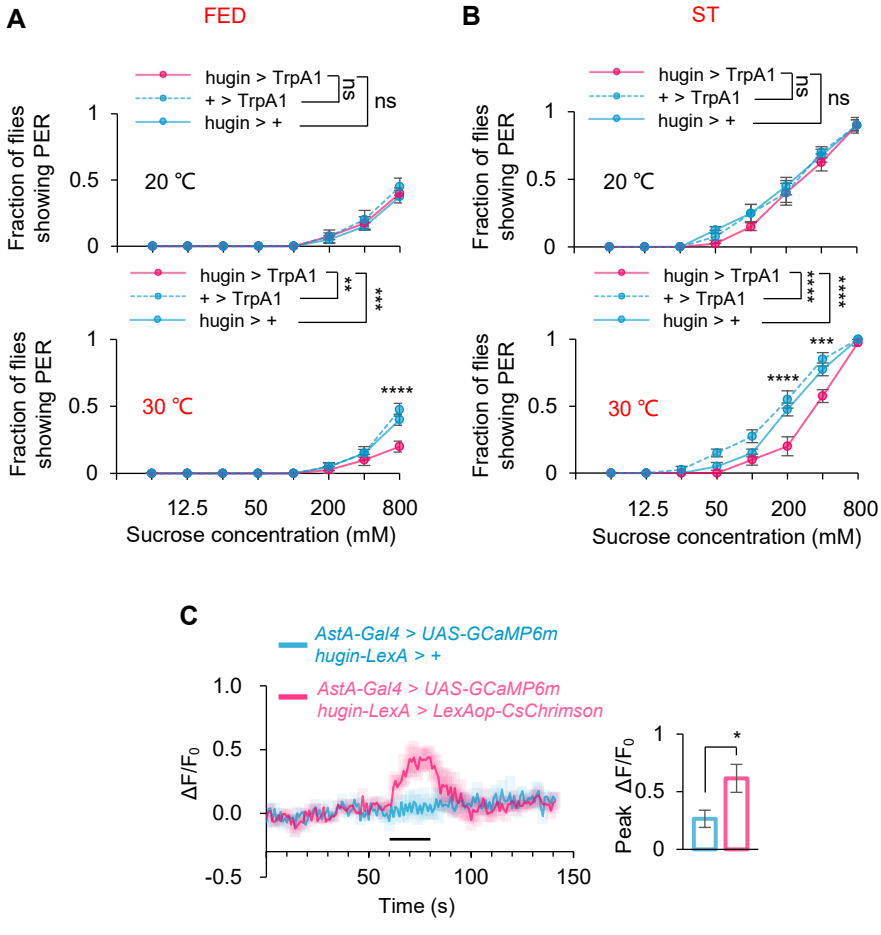

Figure supplementary 12

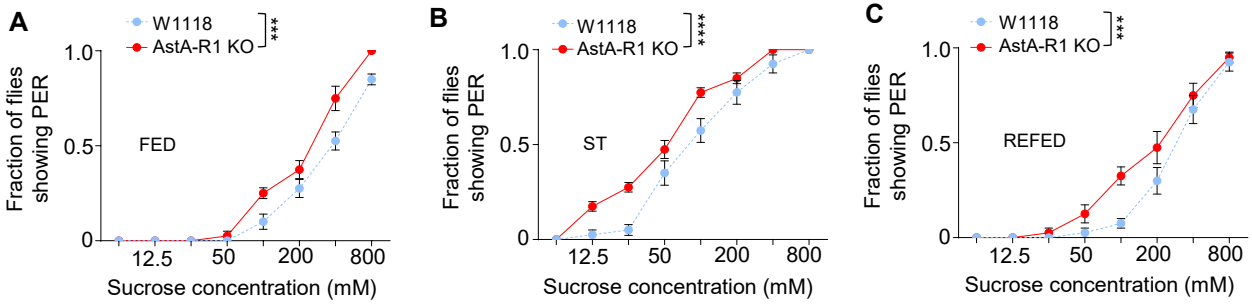

Figure supplementary 13

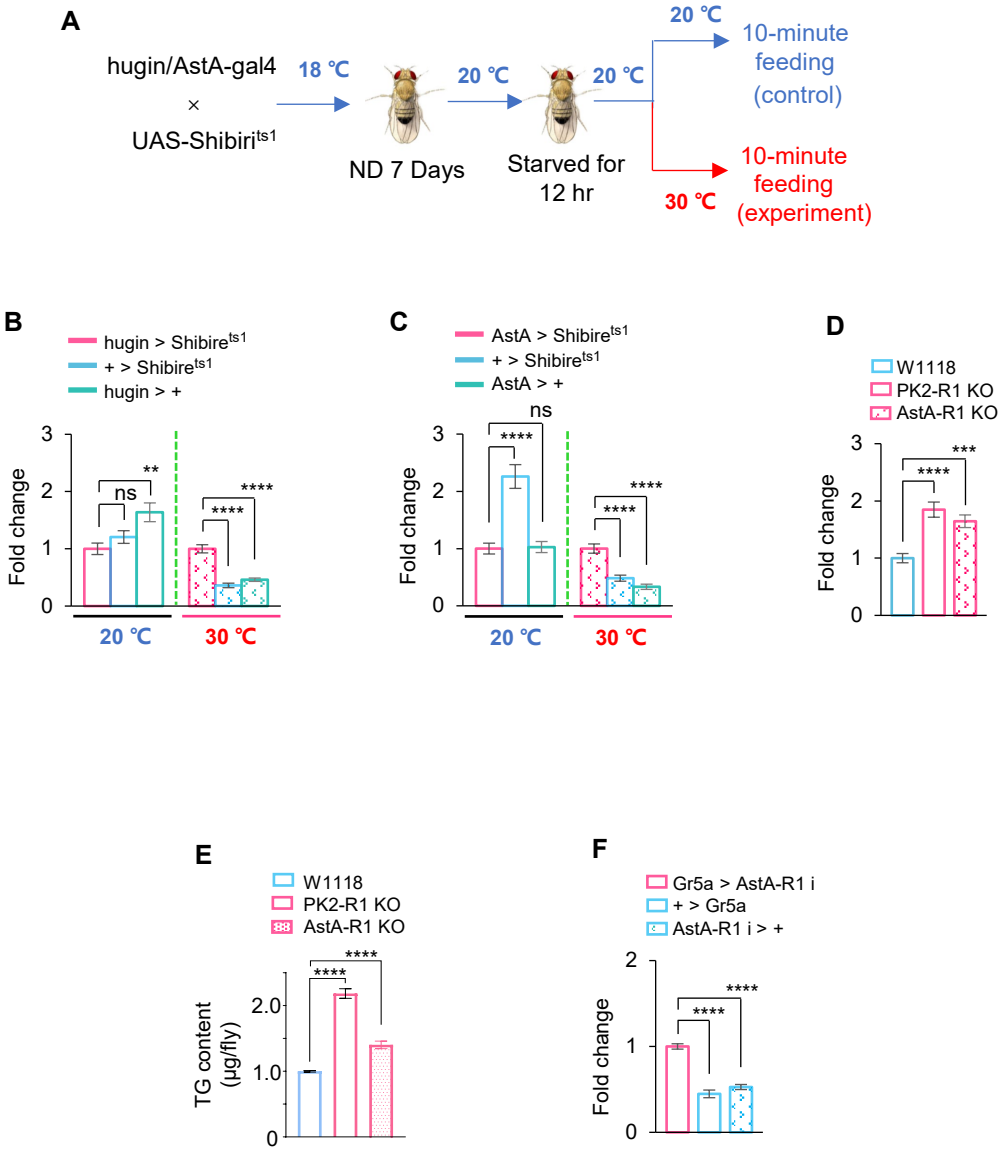

Figure supplementary 14

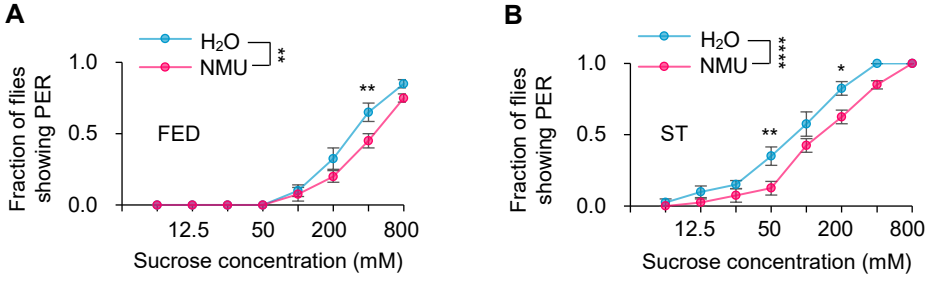

Figure supplementary 15

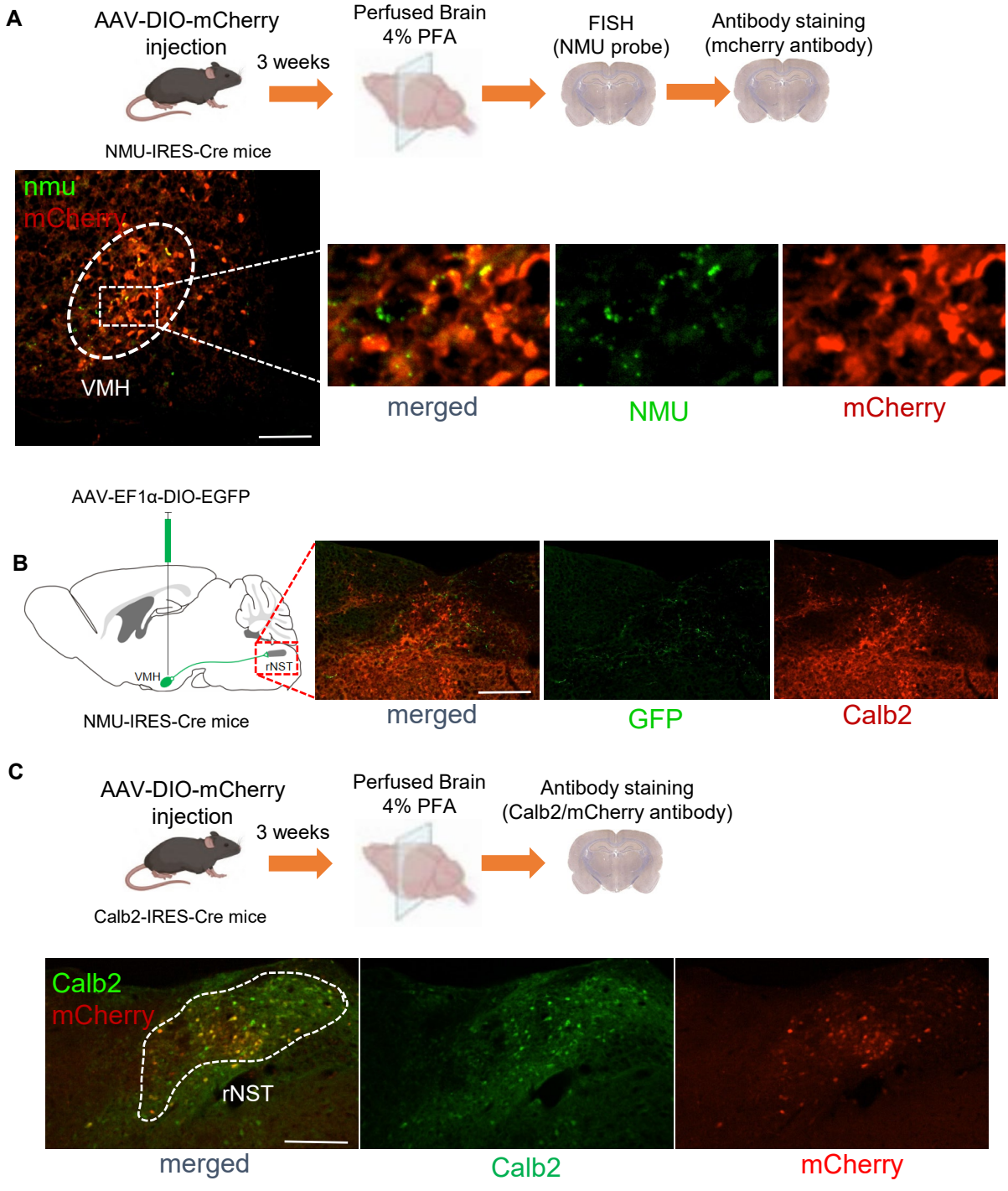
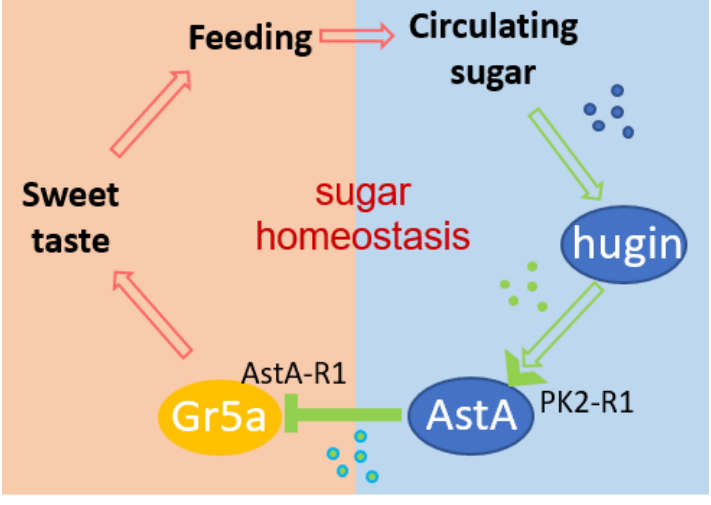
Figure supplementary 16